AGU ADVANCING EARTH AND SPACE SCIENCES

Earth and Space Science

RESEARCH ARTICLE
10.1029/2025EA004646

Special Collection:
Observing CO2 from space: A Decade of progress from NASA's Orbiting Carbon Observatories (OCO-2 and OCO-3)

Comparing v11.2 OCO-2 and v11 OCO-3 X_{CO_2} Retrievals With Ground-Based COCCON Measurements

Saswati Das[1,2,3], Mahesh Kumar Sha[4], Darko Dubravica[5], Thomas E. Taylor[6], Matthäus Kiel[1], Joshua L. Laughner[1], Gregory B. Osterman[1], Christopher W. O'Dell[6], Brendan Fisher[1], Robert R. Nelson[1], Carlos Alberti[5], Bianca C. Baier[7], Dimitrios Balis[8], Hartmut Bösch[9], Andre Butz[10], Zhaonan Cai[11], Jia Chen[12], Frédéric Chevallier[13], Alexandru Dandocsi[14], Nicholas M. Deutscher[15,16], Manvendra K. Dubey[17], Dietrich G. Feist[18,19,20], Lena Feld[5], Jonathan E. Franklin[21], Matthias M. Frey[5], Omaira Garcia[22], Elaine Gottlieb[21], Konstantin Gribanov[23], David W. T. Griffith[15], Michel Grutter[24], Frank Hase[5], Eliezer S. Hernández[25,26], Neil Humpage[27,28], Laura T. Iraci[29], Nicole Jacobs[30], Sujong Jeong[31], Pascal Jeseck[32], Tomi Karppinen[33], Rigel Kivi[33], Morgan Lopez[34], Andreas Luther[12], Maria Makarova[35], Moritz Makowski[12], Erin McGee[30], Marios Mermigkas[7,36], Isamu Morino[37], Justus Notholt[9], Hirofumi Ohyama[37], Thomas Panou[8], Hayoung Park[31], Robert Parker[27,28], David F. Pollard[38], Markus Rettinger[39], Sébastien Roche[40], Coleen M. Roehl[41], Constantina Rousogenous[42], Kei Shiomi[43], William R. Simpson[44], Wolfgang Stremme[24], Kimberly Strong[30], Ralf Sussmann[39], Noemie L. Taquet[24,26], Yao Té[32], Chrysanthi Topaloglou[8], Geoffrey Toon[1], Qiansi Tu[9,45], Mihalis Vrekoussis[15,42], Pucai Wang[46,47], Thorsten Warneke[9], Steven C. Wofsy[21], Debra Wunch[30], Minqiang Zhou[11], Elizabeth Spicer[48], Annmarie Eldering[49], Susan Kulawik[50], Abhishek Chatterjee[1,51], and Vivienne H. Payne[1]

[1]Jet Propulsion Laboratory, California Institute of Technology, Pasadena, CA, USA, [2]NASA Goddard Space Flight Center, Greenbelt, MD, USA, [3]University of Maryland, Baltimore, MD, USA, [4]Royal Belgian Institute for Space Aeronomy, Brussels, Belgium, [5]Institute of Meteorology and Climate Research Atmospheric Trace Gases and Remote Sensing, Karlsruhe Institute of Technology, Karlsruhe, Germany, [6]Cooperative Institute for Research in the Atmosphere, Colorado State University, Fort Collins, CO, USA, [7]NOAA Global Monitoring Laboratory, Boulder, CO, USA, [8]Laboratory of Atmospheric Physics, Department of Physics, Aristotle University of Thessaloniki, Thessaloniki, Greece, [9]Institute of Environmental Physics, University of Bremen, Bremen, Germany, [10]Institute of Environmental Physics, University of Heidelberg, Heidelberg, Germany, [11]State Key Laboratory of Atmospheric Environment and Extreme Meteorology, Institute of Atmospheric Physics, Chinese Academy of Sciences, Beijing, China, [12]Technical University of Munich, Munich, Germany, [13]Laboratoire des Sciences du Climat et de l'Environnement/IPSL, Université Paris-Saclay, Paris, France, [14]National Institute of Research and Development for Optoelectronics, Magurele, Romania, [15]Institute of Environmental Physics (IUP), University of Bremen, Bremen, Germany, [16]University of Wollongong, Wollongong, NSW, Australia, [17]Los Alamos National Laboratory, Los Alamos, NM, USA, [18]Max Planck Institute for Biogeochemistry, Jena, Germany, [19]Lehrstuhl für Physik der Atmosphäre, Ludwig-Maximilians-Universität München, Munich, Germany, [20]Deutsches Zentrum für Luft- und Raumfahrt, Institut für Physik der Atmosphäre, Munich, Germany, [21]Harvard John A. Paulson School of Engineering and Applied Sciences, Harvard University, Cambridge, MA, USA, [22]Izaña Atmospheric Research Center, State Meteorological Agency of Spain (AEMet), Tenerife, Spain, [23]Ural Federal University, INSMA CEPL, Yekaterinburg, Russia, [24]Instituto de Ciencias de la Atmósfera y Cambio Climático, Universidad Nacional Autónoma de México, México City, México, [25]State Meteorological Agency of Spain (AEMET), Santa Cruz de Tenerife, Spain, [26]TRAGSATEC, Madrid, Spain, [27]National Centre for Earth Observation, University of Leicester, Leicester, UK, [28]School of Physics and Astronomy, University of Leicester, Leicester, UK, [29]Atmospheric Science Branch, NASA Ames Research Center, Moffett Field, CA, USA, [30]Department of Physics, University of Toronto, Toronto, ON, Canada, [31]Department of Environmental Planning, Graduate School of Environmental Studies, Seoul National University, Seoul, South Korea, [32]Sorbonne Université, CNRS, MONARIS, UMR8233, Paris, France, [33]Finnish Meteorological Institute, Sodankylä, Finland, [34]Laboratoire des Sciences du Climat et de l'Environnement, Gif-sur-Yvette, France, [35]Department of Atmospheric Physics–1, Faculty of Physics, Saint Petersburg State University (SPbU), Saint Petersburg, Russia, [36]Now at Institute for Astronomy, Astrophysics, Space Applications and Remote Sensing, National Observatory of Athens, Athens, Greece, [37]National Institute for Environmental Studies (NIES), Tsukuba, Japan, [38]National Institute of Water and Atmospheric Research, Lauder, New Zealand, [39]Karlsruhe Institute of Technology (KIT), Institute of Meteorology and Climate Research (IMK-IFU), Garmisch-Partenkirchen, Germany, [40]Environmental Defense Fund, New York, NY, USA, [41]California Institute of Technology, Pasadena, CA, USA, [42]Climate and Atmosphere Research Centre (CARE-C), The Cyprus Institute, Nicosia, Cyprus, [43]Earth Observation Research Center (EORC), Japan Aerospace Exploration Agency (JAXA), Tsukuba, Japan, [44]Department of Chemistry, Biochemistry, and Geophysical Institute, University of Alaska Fairbanks, Fairbanks, AK, USA, [45]School of Mechanical Engineering, Tongji University, Shanghai, China, [46]LAGEO, the Institute of Atmospheric Physics, Chinese Academy of Sciences, Beijing, China, [47]University of Chinese Academy of

Key Points:

- The latest X_{CO_2} data versions from the Orbiting Carbon Observatory (OCO-2/3) missions are evaluated against ground-based observations
- Comparisons against the COllaborative Carbon Column Observing Network (COCCON) include new global sites, extending data evaluation efforts
- Aggregated bias-corrected and quality-filtered X_{CO_2} data from OCO-2/3 agree best with v1 COCCON in the land nadir/glint mode globally

Supporting Information:

Supporting Information may be found in the online version of this article.

Correspondence to:

S. Das,
sdas7@umbc.edu

Citation:

Das, S., Sha, M. K., Dubravica, D., Taylor, T. E., Kiel, M., Laughner, J. L., et al. (2026). Comparing v11.2 OCO-2 and v11 OCO-3 X_{CO_2} retrievals with ground-based COCCON measurements. *Earth and Space Science*, *13*, e2025EA004646. https://doi.org/10.1029/2025EA004646

Received 29 JUL 2025
Accepted 28 MAY 2026

Sciences, Beijing, China, [48]University of Oklahoma, Norman, OK, USA, [49]National Institute of Standards and Technology (NIST), Gaithersburg, MD, USA, [50]Bay Area Environmental Research Institute, NASA Ames Research Center, Mountain View, CA, USA, [51]Now at Schmidt Sciences, New York, NY, USA

Abstract The Orbiting Carbon Observatory-2 and -3 (collectively termed "OCO-2/3," hereafter) missions, together, provide precise and accurate global data records that contribute to a better understanding of the variability in atmospheric carbon dioxide (CO_2). The retrieval algorithm used to process the satellite data, Atmospheric Carbon Observations from Space (ACOS), continues to be updated. The latest v11.2 OCO-2 and v11 OCO-3 data releases include significant improvements compared to past data versions. The Total Carbon Column Observing Network (TCCON), a network of ground-based Fourier Transform Spectrometers (FTS), has historically, been the validation data source for OCO-2/3. The COllaborative Carbon Column Observing Network (COCCON), an emerging network of ground-based portable Fourier Transform Infrared Spectrometers (EM27/SUN), aids satellite validation efforts by providing observations in geographic locations where there are no TCCON measurements being made. This study provides the first global comparison between the OCO-2/3 data sets and the COCCON observations. Currently, the COCCON data set, most useful for global analysis, is version 1 (v1), which our analysis shows is typically lower than the satellites by ∼0.50–1.00 ppm, with scatter against OCO-2/3 roughly similar to TCCON versus OCO-2/3. This analysis includes comparisons of results from the latest v2.x COCCON data version for the sites with the data available. Comparisons with the v2.x COCCON data version generally show improved comparisons against OCO-2/3. Our analysis illustrates the ways in which the COCCON data set, used globally, regionally, or in specific locations, can provide insight into the quality of satellite observations of atmospheric CO_2.

Plain Language Summary The Orbiting Carbon Observatory-2 (OCO-2) and -3 (OCO-3) (collectively referred to as OCO-2/3) are NASA missions that study atmospheric carbon dioxide (CO_2) globally with a high degree of precision and accuracy. Measurements from the Total Carbon Column Observing Network (TCCON), a global network of ground-based Fourier Transform Spectrometers (FTS) dedicated to measuring the column-averaged concentrations of GHGs (including CO_2), have been historically used for validation of satellite observations. The new COllaborative Carbon Column Observing Network (COCCON) complements TCCON by expanding the network of ground-based CO_2 measurements using portable and cost-effective FTSs. We provide the first global comparison between OCO-2/3 with COCCON observations to evaluate the mean differences between the ground- and space-based data sets and identify regions where these differences are most pronounced. Global comparisons suggest bias values (in ppm) of 0.42 (0.03), 0.94 (0.18), 0.88 (−0.01) for OCO-2, and 0.65 (0.03), 0.95 (0.09), 0.67 (0.16) for OCO-3 in the land nadir/glint, ocean glint, and target modes, respectively, against version (v) 1 COCCON, with corresponding values against TCCON listed within the parentheses. For sites with v2.x COCCON data available, reduced biases are observed against OCO-2/3, suggesting the need to update the data at all COCCON sites using the latest PROFFAST v2.4.

1. Introduction

Carbon dioxide (CO_2) is a primary driver of global warming due to its ability to absorb longwave infrared (IR) radiation. Rising CO_2 concentrations globally caused by anthropogenic activities have led to unprecedented changes in the global climate. Thus, precise, accurate, and continuous measurements of atmospheric CO_2 are pivotal in understanding its sources and sinks, predicting future climate scenarios, and developing necessary mitigation strategies.

Remote sensing retrievals of CO_2 from space by satellite instruments have been providing global observations for over 20 years, contributing to a better understanding of the global carbon cycle. The SCanning Imaging Absorption SpectroMeter for Atmospheric CHartographY (SCIAMACHY; Bovensmann et al., 1999), launched by the European Space Agency (ESA) in 2002, became the world's first satellite to retrieve global concentrations of CO_2. Subsequently, the Greenhouse Gases Observing SaTellite (GOSAT) (Kuze et al., 2009, 2016; Yokota et al., 2009), a joint mission by the Japan Aerospace Exploration Agency (JAXA), the Japanese National Institute for Environmental Studies (NIES), and the Japanese Ministry of the Environment (MOE), was launched in January 2009. The GOSAT mission began retrieving global concentrations of CO_2 and methane (CH_4) (Kohtake et al., 2008; Parker et al., 2020). GOSAT retrieves CO_2 with a precision of ∼1–1.5 ppm over land and ∼1 ppm in

Author Contributions:
Conceptualization: Saswati Das
Data curation: Mahesh Kumar Sha, Darko Dubravica, Carlos Alberti, Bianca C. Baier, Dimitrios Balis, Hartmut Bösch, Andre Butz, Zhaonan Cai, Jia Chen, Frédéric Chevallier, Alexandru Dandocsi, Nicholas M. Deutscher, Manvendra K. Dubey, Dietrich G. Feist, Lena Feld, Jonathan E. Franklin, Matthias M. Frey, Omaira Garcia, Elaine Gottlieb, Konstantin Gribanov, David W. T. Griffith, Michel Grutter, Frank Hase, Eliezer S. Hernández, Neil Humpage, Laura T. Iraci, Nicole Jacobs, Sujong Jeong, Pascal Jeseck, Tomi Karppinen, Rigel Kivi, Morgan Lopez, Andreas Luther, Maria Makarova, Moritz Makowski, Erin McGee, Marios Mermigkas, Isamu Morino, Justus Notholt, Hirofumi Ohyama, Thomas Panou, Hayoung Park, Robert Parker, David F. Pollard, Markus Rettinger, Sébastien Roche, Coleen M. Roehl, Constantina Rousogenous, Kei Shiomi, William R. Simpson, Wolfgang Stremme, Kimberly Strong, Ralf Sussmann, Noemie L. Taquet, Yao Té, Chrysanthi Topaloglou, Geoffrey Toon, Qiansi Tu, Mihalis Vrekoussis, Pucai Wang, Thorsten Warneke, Steven C. Wofsy, Debra Wunch, Minqiang Zhou
Formal analysis: Saswati Das, Thomas E. Taylor
Funding acquisition: Abhishek Chatterjee, Vivienne H. Payne
Investigation: Saswati Das
Methodology: Saswati Das, Mahesh Kumar Sha, Matthäus Kiel, Joshua L. Laughner, Gregory B. Osterman, Christopher W. O'Dell
Project administration: Abhishek Chatterjee, Vivienne H. Payne
Resources: Gregory B. Osterman
Supervision: Gregory B. Osterman
Validation: Saswati Das, Matthäus Kiel, Joshua L. Laughner, Gregory B. Osterman, Christopher W. O'Dell
Visualization: Saswati Das, Thomas E. Taylor
Writing – original draft: Saswati Das, Christopher W. O'Dell
Writing – review & editing: Mahesh Kumar Sha, Darko Dubravica, Thomas E. Taylor, Matthäus Kiel, Joshua L. Laughner, Christopher W. O'Dell, Brendan Fisher, Robert R. Nelson, Carlos Alberti, Bianca C. Baier, Dimitrios Balis, Hartmut Bösch, Andre Butz, Zhaonan Cai, Jia Chen, Frédéric Chevallier, Alexandru Dandocsi, Nicholas M. Deutscher, Manvendra K. Dubey, Dietrich G. Feist, Lena Feld, Jonathan E. Franklin, Matthias M. Frey, Omaira Garcia, Elaine Gottlieb, Konstantin Gribanov, David W. T. Griffith, Michel Grutter, Frank Hase, Eliezer S. Hernández, Neil Humpage, Laura T. Iraci, Nicole Jacobs, Sujong Jeong, Pascal Jeseck, Tomi Karppinen, Rigel Kivi,

Morgan Lopez, Andreas Luther, Maria Makarova, Moritz Makowski, Erin McGee, Marios Mermigkas, Isamu Morino, Justus Notholt, Hirofumi Ohyama, Thomas Panou, Hayoung Park, Robert Parker, David F. Pollard, Markus Rettinger, Sébastien Roche, Coleen M. Roehl, Constantina Rousogenous, Kei Shiomi, William R. Simpson, Wolfgang Stremme, Kimberly Strong, Ralf Sussmann, Noemie L. Taquet, Yao Té, Chrysanthi Topaloglou, Geoffrey Toon, Qiansi Tu, Mihalis Vrekoussis, Pucai Wang, Thorsten Warneke, Steven C. Wofsy, Debra Wunch, Minqiang Zhou, Elizabeth Spicer, Annmarie Eldering, Susan Kulawik, Abhishek Chatterjee, Vivienne H. Payne

the ocean-glint observation mode and has a spectral resolution of 0.24 nm (Butz et al., 2011). The GOSAT-2 mission, launched in 2018, retrieves CO_2 with a precision of 0.5 ppm. The Chinese Carbon Dioxide Observation Satellite (TanSat) (Liu et al., 2018; Yang et al., 2018), launched in 2016 by the China National Space Administration (CNSA), monitors global CO_2 levels (Wang et al., 2020). It has a spectral resolution of ∼0.1 nm and a broad range of applications.

The Orbiting Carbon Observatory-2 (OCO-2) (Crisp et al., 2004, 2006, 2008) mission, launched by NASA on 2 July 2014, represents a significant advancement in the remote sensing of atmospheric CO_2. OCO-2's primary objectives include observing global CO_2 levels with exceptional precision and accuracy (Crisp et al., 2017; Thompson et al., 2012), identifying CO_2 sources and sinks (Philip et al., 2022; Shekhar et al., 2020; Villalobos et al., 2021), studying patterns of seasonal and interannual variability in atmospheric CO_2 (Kunchala et al., 2022; Philip et al., 2022; X. Guan et al., 2024; Y. Guanet al., 2024; R. Lei et al., 2024), improving climate models and their predictive capabilities by supplying crucial data (Miller et al., 2018; Patra et al., 2021), and providing reliable data to inform climate change mitigation and policies (Nassar et al., 2021; T. T. Lei et al., 2024). OCO-2 is equipped with three high-resolution grating spectrometers that measure the intensity of sunlight reflected off the Earth's surface at specific wavelengths absorbed by CO_2. These spectrometers operate in three narrow spectral bands in the near-infrared (NIR) and short-wave infrared (SWIR) regions. The band centered at 0.76 μm (μm) measures molecular oxygen (O_2) and provides information on the total column of air being observed. It is also used to calculate the dry-air mole fraction of CO_2 (X_{CO_2}), which is an important quantity in carbon cycle science due to its relative insensitivity to vertical mixing and its direct utility in the quantification of CO_2 surface fluxes (Keppel-Aleks et al., 2011; Yang et al., 2007). The spectral band centered at 1.61 μm, referred to as the weak CO_2 band, provides information on the CO_2 concentrations. The strong CO_2 band, less influenced by aerosol scattering, is centered at 2.06 μm. OCO-2's spectrometers operate with a spectral resolution of 0.1 nm (nm), significantly higher than those of GOSAT, Sentinel-5 Precursor, and TanSat. This high spectral resolution enables OCO-2 to detect subtle variations in CO_2 concentrations accurately. OCO-2 operates in a sun-synchronous orbit, measuring at a similar local time during its 16-day repeat cycle, reducing diurnal variations and providing a stable data set for long-term trend analysis. Further, OCO-2 provides high spatial resolution, utilizing a push-broom scanning technique having a cross-track swath width of 10 km, with each measurement covering approximately 1.29 km (cross-track) × 2.25 km (along-track).

The Orbiting Carbon Observatory-3 (OCO-3), installed on the International Space Station (ISS) in May 2019, was developed to build upon and enhance the capabilities of its predecessor, OCO-2. OCO-3 provides precise and accurate retrievals/observations of atmospheric CO_2 (Basilio et al., 2019; Eldering et al., 2019; Rosenberg et al., 2020; Taylor et al., 2023). The ISS orbit allows for observations during different times of the day, providing new insights into the temporal and spatial variability of CO_2 sources and sinks and enhancing the understanding of diurnal patterns and short-term variations. Like OCO-2, OCO-3 uses high-resolution grating spectrometers, with a spectral resolution of 0.1 nm, to measure the intensity of sunlight reflected from the Earth's surface in three narrow bands located in the near-infrared region centered at 0.76, 1.61, and 2.06 μm, referred to as the O_2, weak CO_2, and the strong CO_2 bands, respectively. OCO-3's novel pointing mechanism enables "snapshot" area mapping to capture high-resolution images of CO_2 concentrations over specific regions of interest (e.g., forests and urban areas) spanning an 80 km × 80 km area to quantify localized CO_2 sources and sinks.

For both OCO-2 and OCO-3 (collectively termed OCO-2/3, hereafter), the data are reported in terms of X_{CO_2}, the ratio of the CO_2 column abundances to the column of dry air, where the CO_2 column abundance refers to the altitude-dependent number density of CO_2 integrated over the atmospheric column. The Atmospheric Carbon Observations from Space (ACOS) algorithm, described by O'Dell et al. (2012, 2018) and validated extensively in those and other works (Das et al., 2025; Jacobs et al., 2024; Kiel et al., 2019; Taylor et al., 2023; Wunch et al., 2017), is used to retrieve the column abundance of CO_2 from high-resolution spectra of reflected sunlight. X_{CO_2} retrievals are minimally impacted by localized CO_2 variations, local surface emissions, weather, and short-term fluctuations, provide a more comprehensive view of the CO_2 distribution and are better indicators of the global CO_2 trends. Thus, X_{CO_2} retrievals warrant high precision and accuracy to distinguish them from high background X_{CO_2} concentrations. Due to their long-standing operational history of over five (OCO-3) and ten (OCO-2) years, highly precise and accurate space-based X_{CO_2} retrievals require continuous validation against independent data sets to identify, characterize, and eliminate biases.

The Total Carbon Column Observing Network (TCCON) (Laughner et al., 2024; Wunch et al., 2010, 2011a) is a global network of solar-viewing ground-based Fourier Transform Spectrometers (FTS) dedicated to the precise retrievals of the column-averaged dry-air mole fractions (X_{gas}) of greenhouse gases (GHGs), primarily CO_2, CH_4, and CO. Additionally, column-averaged abundance of O_2, nitrous oxide (N_2O), hydrofluoric acid (HF), water vapor (H_2O), and semi-heavy water (HDO) are also retrieved. With its inception in the early 2000s and the initial instrument deployment in 2004, the TCCON data spans over two decades with 29 active TCCON sites worldwide. With a high spectral resolution of ~0.02 cm^{-1}, the TCCON instruments detect the fine absorption features in the NIR region of the solar spectrum to provide accurate X_{gas} observations. While the TCCON instruments cannot observe through optically thick clouds, they suffer less interference from aerosols and have better control over instrument health than spaceborne instruments. Historically, TCCON has been used as the primary X_{CO_2} validation source for many satellites making measurements of greenhouse gases, including the OCO-2, OCO-3, GOSAT, GOSAT-2, TanSat, and SCIAMACHY missions. A detailed description of the OCO-2/3 retrieval algorithm updates across the many versions and the corresponding evaluations against TCCON have been discussed later in the paper, in the "Data and Retrieval Method" section (Section 2).

The COllaborative Carbon Column Observing Network (COCCON) was established in 2018 to enhance global CO_2 measurement capabilities in response to the growing need for high-quality ground-based observations of CO_2 and other greenhouse gases. Developed at the Karlsruhe Institute of Technology (KIT) in collaboration with Bruker Optics, COCCON coordinates a network of "EM27/SUN" spectrometers. The EM27/SUN is a new generation of portable and easy-to-deploy Fourier Transform Infrared (FTIR) spectrometers (Gisi et al., 2012) to retrieve the column-averaged abundances of CO_2, CH_4, and H_2O. The EM27/SUN instruments are lightweight and relatively low-cost compared to full TCCON stations, and they enable measurements in locations that lack the infrastructure to support a more complex and elaborate TCCON setup. The COCCON EM27/SUN spectrometer has a spectral resolution of 0.5 cm^{-1}, lower than the TCCON spectrometers (0.02 cm^{-1}), but adequate to observe the absorption features of GHGs in the NIR region of the solar spectrum. The COCCON and TCCON measurements complement each other; the lower cost of an EM27/SUN allows for the creation of networks of spectrometers and making measurements in new areas in a way that is particularly valuable for assessing real-time local GHG sources, such as landfills, power plants, and urban emissions. As of 2026, COCCON has expanded, with 40 spectrometers operational across the globe, and planning for the deployment of many more instruments is currently underway. Utilizing this new data resource can provide important insights to satellite missions such as OCO-2/3 X_{CO_2}, particularly in regions where TCCON data might not be available.

The OCO-2/3 X_{CO_2} data are vicariously tied to the World Meteorological Organization (WMO) measurement standard via comparisons to TCCON observations, which in turn are compared to in situ observations that utilize the WMO standard (Das et al., 2025). Wunch et al. (2010), Messerschmidt et al. (2011), and Laughner et al. (2024) described how TCCON X_{CO_2} data are tied to in situ measurements via scale factor derivation by comparing against many in situ vertical profiles (aircraft, balloon-borne) measured over TCCON locations. Because it is difficult to get vertical profiles in all locations, COCCON is linked to the WMO scale through coordinated observations at TCCON sites. KIT maintains an EM27/SUN instrument that is used as a "travel standard" to cross-validate COCCON instruments. It is thus important to ensure that the COCCON and TCCON measurements are harmonized through rigorous scaling and validation procedures conducted at KIT, allowing COCCON to maintain a data quality comparable to TCCON's high-resolution instruments, ensuring COCCON's integration into the larger framework that abides by WMO's GHG observation standards (Alberti et al., 2022; Frey et al., 2019; Herkommer et al., 2024; Sha et al., 2024).

Formerly, for earlier X_{CO_2} data versions, validation using TCCON was performed by Das et al. (2025) and Wunch et al. (2017) for OCO-2, and by Taylor et al. (2023) for OCO-3. Global comparisons of version 11.1 (v11.1) OCO-2 against GGG2020 TCCON X_{CO_2} data, by Das et al. (2025), suggested that the aggregated, bias-corrected, and quality-filtered absolute average bias values are less than 0.20 ppm across all OCO-2 observation modes, with the lowest bias value of -0.03 ± 0.85 ppm in the land nadir/glint mode. This was an update to the findings of Wunch et al. (2017), who estimated that the global bias values, across all OCO-2 observation modes, remained under 0.40 ppm when comparing version 7 OCO-2 against GGG2014 TCCON X_{CO_2} data. Taylor et al. (2023) found bias values less than or equal to 0.12 ppm over land and 0.09 ppm over ocean for version 10.4 OCO-3 compared to GGG2020 TCCON X_{CO_2} data.

Gadhavi et al. (2025), Jacobs et al. (2020), Park et al. (2024), and Sha et al. (2025) used EM27/COCCON measurements of X_{CO_2} (and other atmospheric quantities) to compare against satellite-based measurements from OCO-2, OCO-3, GOSAT, GOSAT-2, and Sentinel-5 Precursor (Veefkind et al., 2012). Version 9 OCO-2 comparisons against COCCON suggested absolute bias values under 1.00 ppm across different seasons at northern high-latitude regions (Jacobs et al., 2020). Park et al. (2024) suggested that OCO-2/3 show a bias of 0.44% ± 0.24% compared to the EM27/SUN over Seoul, while GOSAT and GOSAT-2 show a bias of 1.04% ± 0.74% and 0.42% ± 0.49%, respectively. Gadhavi et al. (2025) reported bias values less than 0.50 and 0.70 ppm, respectively, for v11.1 OCO-2 and version 3.05 (v3.05) GOSAT against EM27/SUN X_{CO_2} measurements in India. Over land, the bias values, as reported by Sha et al. (2025), were 0.24 and 0.65 ppm, respectively, for v11.1 OCO-2 and v3.05 GOSAT against v1 COCCON. Wei et al. (2022) analyzed EM27/SUN data against space-based X_{CO_2} retrievals in Western China. They found the bias values (satellite instrument–EM27/SUN) to be −0.34 ppm, typically 1.50, 1.77, and 1.59 ppm, respectively, for GOSAT, GOSAT-2, OCO-2, and OCO-3.

Previous studies by Frey et al. (2019) and Sha et al. (2024) provided comparative results of the TCCON and COCCON data sets. Frey et al. (2019) compared the EM27/SUN data at Karlsruhe against truncated Infrared Fourier Spectrometer (IFS) 125 High-Resolution (125HR, Bruker Optics GmbH & Co. KG, Ettlingen, Germany) data derived from full-resolution TCCON interferograms (to eliminate sensitivity-dependent artifacts) and found a bias of 0.60 ppm for X_{CO_2}. Sha et al. (2020) reported a mean X_{CO_2} bias of −0.18 ppm between the EM27/SUN instrument and TCCON at Karlsruhe. Alberti et al. (2022) described the extended COCCON calibration procedures and the incorporation of refined methods, and compared TCCON and COCCON data at Karlsruhe, suggesting reasonable agreement with no drifts in the data. Sha et al. (2024) reported the mean X_{CO_2} bias between EM27/SUN and TCCON data at Sodankylä to be −0.72 ppm.

In adherence to the WMO's GHG observation standards, the OCO-2/3 data are scaled to match coincident TCCON measurements, ensuring that the OCO-2, OCO-3, TCCON, and COCCON data sets are compatible. The OCO-2/3 data sets are bias corrected using different methods and ancillary data, including TCCON data. The different methods of bias correction are used to achieve global bias correction, but also to check how the bias correction works on regional scales. The different bias correction methods, discussed later in the paper, provide consistent results. While some of the TCCON data are used in the bias correction, we have determined that the data can still be used for validation. More information about the bias correction process for OCO-2/3 can be found in the OCO-2/3 Data User Guide (DUG) (OCO-2/3 DUG, 2024). Note that while the TCCON network has been rigorously validated, the growing COCCON network is subject to further validation. Therefore, this work aims to compare (rather than validate) the ground-based measurements from COCCON against the space-based measurements from OCO-2/3, with an understanding of the uncertainties associated with either data set. This work also provides the latest OCO-2/3 data validation against the TCCON GGG2020 data set in the Supporting Information S1, in light of the OCO-2/3 versus COCCON comparisons.

In this study, we use the latest version of the bias-corrected and quality-filtered satellite X_{CO_2} observations, version 11.2 (v11.2) for OCO-2 and version 11 (v11) for OCO-3, and compare against coincident measurements from COCCON. The comparisons are done globally using COCCON version 1 (v1) data and locally with version 2 (v2) for selected sites where the data are available. The v11.2 OCO-2 data are used from September 2014 to March 2024, and the v11 OCO-3 data are used from August 2019 to November 2023. The data sets and retrieval method are shown in Section 2, the coincidence criteria are discussed in Section 3, the OCO-2/3 versus v1 COCCON (global comparison) results are shown in Section 4, the OCO-2/3 versus v2 COCCON (comparison over selected sites) results are shown in Section 5, and the conclusions are discussed in Section 6.

2. Data and Retrieval Method

2.1. OCO-2

With OCO-2's launch in 2014, the first release of the OCO-2 data established the baseline version of the ACOS algorithm used for retrieving the X_{CO_2} products. OCO-2 has been operational for over a decade and has consistently recorded rising X_{CO_2} values, discussed in detail in the Supporting Information S1. Over the course of the mission, the instrument/radiometric calibration and other retrieval algorithm processes have been updated and improved, leading to new releases of the OCO-2 data products. Validation against ground-based measurements has been performed continuously throughout the mission. Over the course of the mission, refinements were

introduced to the ACOS algorithm to enhance cloud and aerosol corrections that aimed to minimize errors in X_{CO_2} retrievals. In the v7 OCO-2 data, the algorithm was optimized, and additional refinements were made to the retrieval algorithm to improve its performance across various atmospheric conditions. Wunch et al. (2017) validated the v7 OCO-2 data by performing systematic comparisons to TCCON. Several major algorithms and calibration changes have been implemented to improve the OCO-2 retrievals since v7. The v8 OCO-2 data implemented refined empirical bias correction based on more recent comparisons with TCCON measurements, updated spectroscopic parameters, accounted for stratospheric aerosols, improved surface reflectance treatment in the Level 2 (L2) algorithm, and updated radiometric calibration of the Level 1B (L1B) product (O'Dell et al., 2018). The v9 OCO-2 data product (Kiel et al., 2019) mitigated topography-related biases in X_{CO_2} present in v7 and v8. These biases originated from errors in relative surface pressure estimates caused by OCO-2 detector pointing errors, which propagated nearly 1:1 into bias-corrected X_{CO_2} retrieval errors. Additionally, errors in the re-sampling method used to derive the a priori surface pressure from meteorological re-analysis data affected the retrieval accuracy. Both sources of error were addressed in v9. The v10 OCO-2 product included important changes in the calibration methods, ensuring consistency and reliability across different atmospheric conditions. In this version, the L1B calibration was updated, accounting for radiometric degradation and bad pixel samples (Taylor et al., 2023). The treatment of surface albedos, the solar continuum model, the a priori information for aerosols and CO_2, and the trace gas spectroscopic parameters used in the retrieval algorithm were updated.

V11.2 is a new lite file sub-version of the v11 OCO-2 data product (Das et al., 2025). Jacobs et al. (2024) provided a detailed description of the spectroscopy updates, improved ocean surface treatment, the addition of new a priori profiles, and modifications to sounding selection-governing rules. In transitioning from v11 to v11.1, a new Digital Elevation Map (DEM) was implemented in the L2 retrievals. This is used as a post-processing correction in the v11.1 "Lite" processing, explained in the OCO-2/3 DUG. The most recent v11.2 implements refined radiative transfer modeling that improves the models to provide robust, better estimates of the aerosol and cloud scattering effects, enhancing the robustness of the X_{CO_2} retrievals and the enhanced empirical bias correction. A change in the GEOS5 FP product necessitated an update to the meteorological prior source that included the addition of nitrate aerosols and adjustments to the necessary meteorological parameters, such as the surface pressure and temperature profiles.

This study uses the OCO-2 L2 release v11.2 OCO-2 "Lite" files. The L2 Lite files come with post-processing data fields, including screened and bias-corrected X_{CO_2} values. The "xco2_quality_flag," when set to 0, helps filter for "good quality soundings" only. The OCO-2/OCO-3 DUG (2024) provides the parameters used in the land and ocean bias correction and the overall v11.2 bias-correction process. Furthermore, it describes how potential drifts in the retrieved X_{CO_2} have been checked, given OCO-2's long-standing data record. A linear least squares fit of the monthly mean difference (ΔX_{CO_2}) between the OCO-2 and Truth data sets, accounting for averaging kernel effects, was performed to identify any spurious time-driven trends. Although the current bias correction does not include a time-dependent term, no statistically significant time drift has been observed so far. As OCO-2's data record continues to grow, monitoring and addressing any potential spurious time trends will be essential in the future.

The National Oceanic and Atmospheric Administration (NOAA) Global Monitoring Laboratory (GML) is the WMO GAW (Global Atmospheric Watch) central calibration laboratory for atmospheric CO_2 trace gas standards. It is thus important that all atmospheric CO_2 measurements adhere to the WMO standards for increasing compatibility of global observations. The WMO CO_2 calibration scale revisions indicate enhancements on the order of 0.2 ppm in CO_2 mole fractions at 400 ppm (Hall et al., 2021), and this change must translate into in situ CO_2 measurements via recalibration and remotely sensed CO_2 data through reevaluation against the updated in situ data. The new scale is termed "WMO-CO_2-X2019" (hereafter X2019). The v11.2 OCO-2 data files, like v11.1, consist of an additional variable, "XCO2_X2019," that provides X_{CO_2} estimates on the X2019 scale. The "TCCON_ADJUST" value was re-fitted from 0.9997 for the X2007 scale to 0.9995 for the X2019 scale. This resulted in an enhancement of ~0.08 ppm in the X_{CO_2} values from the X2007 to the X2019 scale (OCO-2/OCO-3 DUG, 2024). The results discussed in this paper (and the Supporting Information S1) compare the OCO-2 data on the X2019 scale against coincident COCCON data. The OCO-2 observation modes and comparisons against TCCON GGG2020 have been discussed in Supporting Information S1.

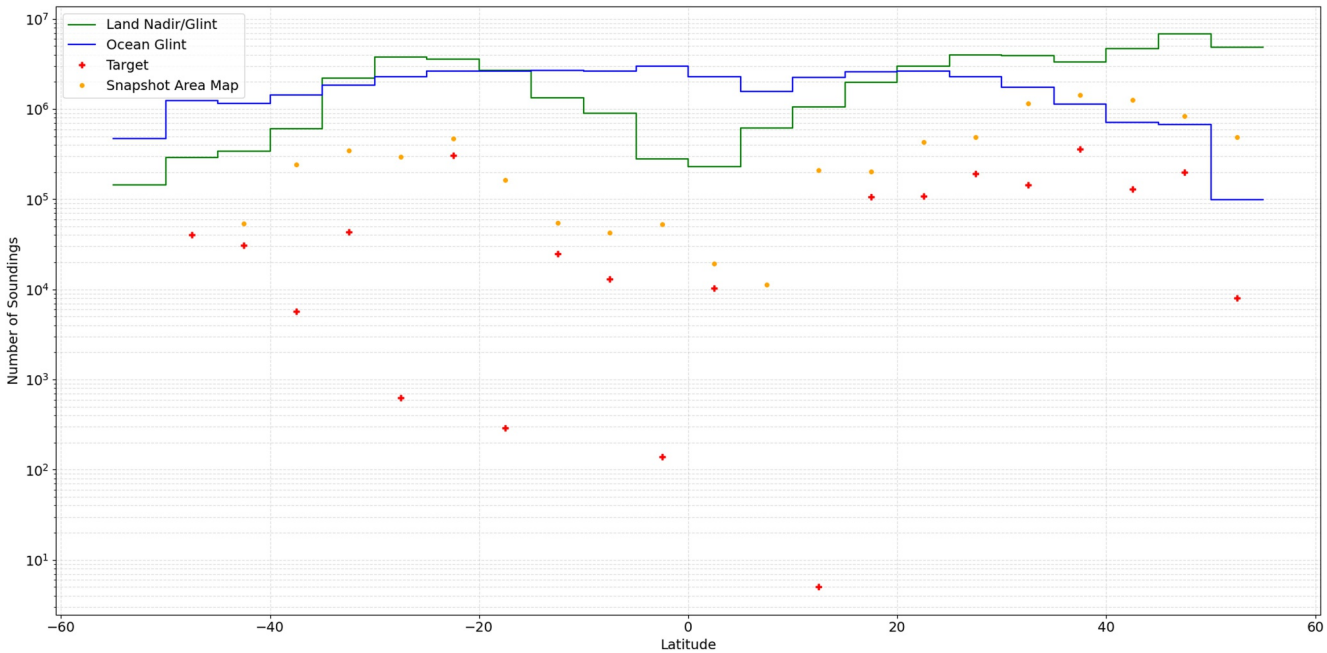

Figure 1. OCO-3 land nadir/glint, ocean glint, target-mode and snapshot area map measurement density in 5° bins as a function of latitude from August 2019 to November 2023, plotted using data from OCO-3 v11 "lite" files for "xco2_quality_flag" set to 0.

2.2. OCO-3

OCO-3 was launched in 2019 and is located on the ISS, with vEarly being the first released OCO-3 data version that focused on integrating and testing the core systems and algorithms derived from OCO-2 but adapted for the unique orbital and pointing characteristics of the ISS (Basilio et al., 2019; Bell et al., 2023; Eldering et al., 2019; Kiel et al., 2021; Taylor et al., 2023). This was followed by v10, in which the radiometric calibration was significantly improved compared to its predecessor, and the lamp data across the entire mission were processed using a consistent set of algorithms. The v10 OCO-3 was succeeded by the v10.4r "Lite" products, where "*r*" indicates the retrospective data (OCO-2/OCO-3 DUG, 2022, 2023).

In the latest v11 OCO-3, the calibration was improved along with substantially better pointing knowledge (Keller et al., 2025). The algorithm was enhanced to include spectroscopy updates to the version 5.2 absorption coefficient model (hereafter, ABSCO (Oyafuso et al., 2017) v5.2), the change of the DEM to Copernicus DEM (Jacobs et al., 2024), prior meteorology updated from GEOS-FPIT to GEOS IT, and other minor updates (Jacobs et al., 2024). The v11 OCO-3 training data sets used five truth proxies for the filtering and bias-correction: (a) Multi-Model-Median, (b) TCCON (GGG2020), (c) Small Area Approximation, (d) OCO-2 Collocations, and (e) Coastal Crossings. The land and ocean X_{CO_2} quality filters are based on 23 variables, consistent with older OCO-3 data versions. The land bias correction used newly derived parametric bias correction coefficients, fixed footprint bias correction, a bias linear in zero-level offset (ZLO, relevant to data earlier than 12 January 2021), and a Global Scaling Factor to tie v11 X_{CO_2} to TCCON. The bias correction for ocean data used different variables than land data, and the ocean global scaling was tied to land via coastline crossings. These updates have been explained in detail in the OCO-2/OCO-3 DUG (2024). The results discussed in this paper compare the OCO-3 data on the X2019 scale against coincident COCCON data. The OCO-3 comparisons against TCCON GGG2020 have been discussed in Supporting Information S1. Figure 1 shows the OCO-3 measurement density for all observation modes as a function of latitude from August 2019 through November 2023. OCO-3 SAM observations over various ECOsystem Spaceborne Thermal Radiometer Experiment on Space Station (ECOSTRESS, Fisher et al., 2020), fossil (fossil fuel emission sources such as power plants), desert, solar-induced fluorescence (SIF), volcano, campaign, and validation sites, and OCO-3 targets taken over many calibration, fossil, and validation sites are shown in the map in Figure 2.

10.1029/2025EA004646

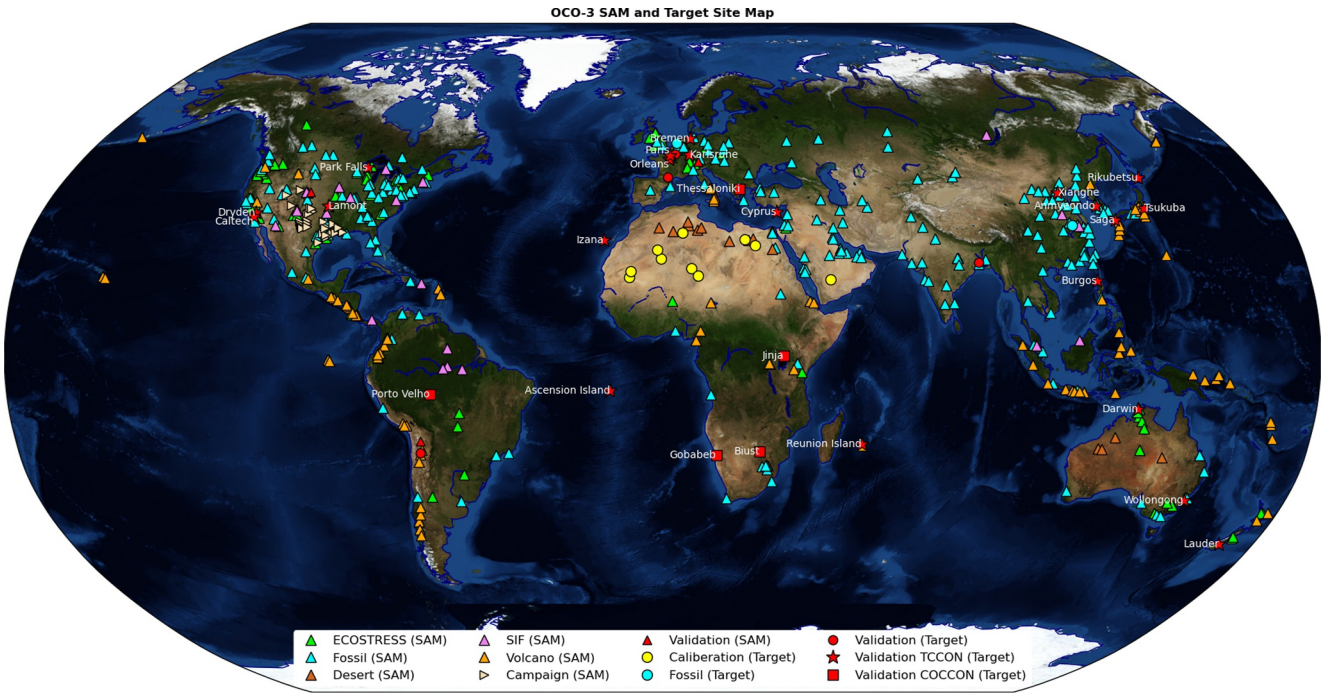

Figure 2. Map of all OCO-3 SAM and target locations. The green, blue, brown, pink, orange, beige, and red triangles indicate SAMs over the ECOSTRESS, fossil, desert, solar-induced fluorescence, volcano, campaign, and validation sites, respectively. The yellow, blue, and red circles indicate the targets over calibration, fossil, and validation sites, respectively. The red star and square indicate the targets taken over TCCON and COCCON sites, respectively. Only SAMs and targets over validation sites have been named on the map and are indicated by red markers.

The TCCON data and a map of the previous, current, and future TCCON sites have been presented in Supporting Information S1.

2.2.1. OCO-3 Observation Modes

The nominal viewing strategy of OCO-3 is similar to OCO-2, that is, nadir and glint modes. While OCO-2 performs complex maneuvers of the satellite bus to make target measurements, OCO-3's 2-D pointing mechanism (PMA) enables rapid transition between the nadir and glint modes (under a minute) and target mode observations over ground-based validation sites, like TCCON. An additional mode in OCO-3 is the SAM mode, which scans large contiguous areas, in the order of 80 km × 80 km (e.g., cities and forests), over CO_2 emission hotspots, volcanoes, and terrestrial-carbon focus regions on a single overpass. SAMs provide a novel and expansive data set to evaluate GHG emissions and SIF from space. Eldering et al. (2019) described this in detail.

Due to the expansive nature of the OCO-3 Target and SAM list, Table S2 in Supporting Information S1 mentions only the ones where TCCON or COCCON sites are located. The "Target Active Status" column indicates if the target or SAM location is active as of November 2024. Targets and SAMs taken over these ground-based locations were defined, obtaining data for OCO-3 validation. Note that OCO-3 was designed so that it could make SAM observations over a variety of different areas of scientific interest. A centralized and comprehensive list of all OCO-3 targets and SAMs, along with data maps for visualization, can be found on the OCO-3 SAMs webpage (https://ocov3.jpl.nasa.gov/sams/).

2.3. COCCON

COCCON (Alberti et al., 2022; Frey et al., 2019, 2021; Herkommer et al., 2024; Sha et al., 2020; Vogel et al., 2019) utilizes portable and cost-effective spectrometers, the EM27/SUN (Gisi et al., 2012; Hase et al., 2016), to measure column-averaged concentrations of CO, CO_2, CH_4, H_2O, and other atmospheric trace gases. The rapid expansion of COCCON represents a significant advancement in the field of atmospheric GHG monitoring, enhancing global CO_2 coverage, particularly in regions such as Africa, South America, and Asia. The COCCON data are retrieved using the PROFFAST algorithm, an efficient and open-sourced tool developed to

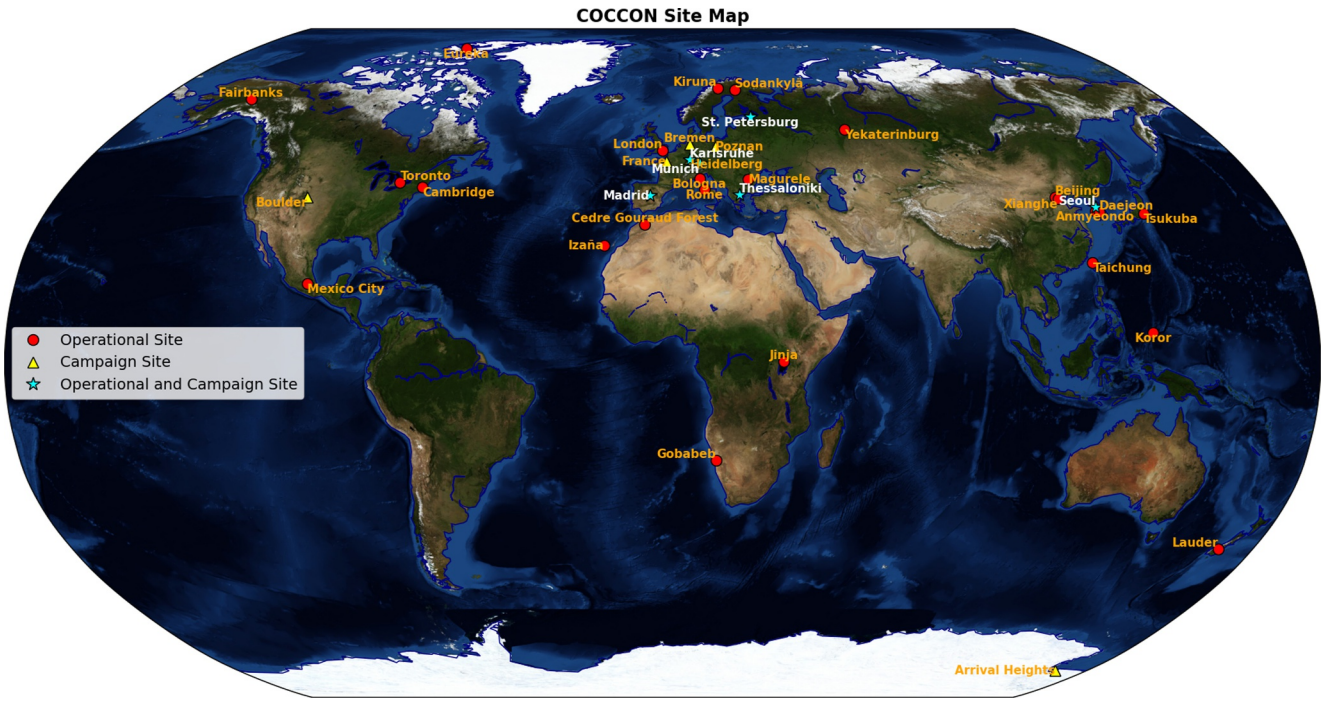

Figure 3. Map of all COCCON stations; red circles, yellow triangles, and blue stars indicate locations with operational, campaign, and both sites, respectively. Mexico City has seven COCCON sites–Altzomoni, Amec, Boxo, Cuat, Tecamac, Unam, and Vallejo.

process solar absorption spectra measured by the EM27/SUN FTIR spectrometers (Sha et al., 2025). Note that PROFFAST is not an acronym but the actual name of the software.

The FTIR measurements are processed and analyzed by preprocessing the raw interferograms to generate spectra, and the absorption spectra are quantitatively analyzed to determine the abundance of the trace gas. The COCCON-PROCEEDS project, supported by the European Space Agency (ESA), developed PREPROCESS, an open-source tool for preprocessing the raw interferograms, and PROFFAST for the retrieval of X_{CO_2}, X_{CO}, X_{CH_4}, and X_{H_2O} in the NIR region. PROFFAST operates by performing a least squares fitting of the spectra, adjusting scaling factors based on a priori profiles of the trace gas. Auxiliary parameters, such as the instrument line shape (ILS), are incorporated using open-path measurements. By the inclusion of ILS parameters, the scatter is reduced in the results across different instruments by the algorithm, introducing consistency in the retrievals throughout the network. This is important for enhancing the accuracy of the results during side-by-side EM27/SUN measurements. Furthermore, initial data conditioning before the analysis is handled by the algorithm that runs simultaneously with the PREPROCESS code (Alberti et al., 2022; Pollard, Hase, et al., 2022; Pollard, Robinson, et al., 2022). COCCON X_{CO_2} data using PROFFAST v1 have been used in this paper. Note that PROFFAST v2.4 is currently available, but only for a few selected sites at the time of this analysis. Therefore, for the sake of maximizing the amount of data to create a global data set, COCCON data processed using PROFFAST v1 have been used in this analysis. This allowed us to minimize the site-to-site biases in the OCO-2/3 versus COCCON results attributable to the use of data processed using different PROFFAST versions. The v2.x COCCON data, available for limited COCCON sites, are used to compare against the OCO-2/3 data sets, and the results are discussed in Section 5. Note that all sub-versions of v2 COCCON data are collectively termed "v2.x." The PROFFAST v1 and v2.x data analysis schemes aim to match the X2007 scale.

The documentation for all PROFFAST versions, data processing information, and COCCON data for specific sites can be accessed through the KIT website (https://www.coccon.kit.edu/index.php) and hosted by the ESA's atmospheric Validation Data Center (EVDC). A map of all currently operational and campaign COCCON sites is shown in Figure 3 and identified by the markers listed within the parentheses. Note that operational sites such as Anmyeondo, Daejeon, Koror, London, Taichung, and campaign sites such as Ewha University, France, and Poznan do not have their data published, and thus, have not been used in this study. Other operational sites

Table 1
Spatial Coincidence Criteria for the Land Nadir/Glint and Ocean Glint Modes

Site name	Latitude	Longitude
All sites except those listed below	±1.25°	±2.5°
Mexico city area sites (Altzomoni, Amec, Boxo, Cuat, Tecamac, Unam, Vallejo)	±1°	±1°
Beijing	±0.25°	±0.25°
Tsukuba	±0.25°	±0.25°
Xianghe	±0.25°	±0.25°
Seoul	±0.25°	±0.25°

Note. The COCCON stations are centered within the coincidence boxes, with the latitude and longitude sizes specified below. Some sites use tighter spatial collocation to exclude observations from neighboring sites or the surrounding topography effect.

(Bologna and Rome) and campaign sites (Arrival Heights, Heidelberg, and Madrid) did not have enough coincident measurements with OCO-2/3 to be included in this analysis.

Tables S1 and S2 in Supporting Information S1 list the geographic locations and the literature citations for the COCCON (EM27/SUN) data used in this study, which are OCO-2/3 target and/or SAM sites. It should be noted that in the process of bias correcting the X_{CO_2} data, OCO-2 and OCO-3 incorporate some TCCON data in addition to results from other data sets (OCO-2/OCO-3 DUG, 2022, 2023). Therefore, this could contribute to better agreement of OCO-2/3 with TCCON than COCCON. The TCCON data retrievals use GGG2020 a priori profiles, while all v1 COCCON data use GGG2014 a priori profiles. Since the v2.x COCCON data were processed individually by the COCCON data-providing institutions; the a priori profiles vary between GGG2014 and GGG2020 from site to site. Note that the v11.2 OCO-2/v11 OCO-3 priors are close to the TCCON GGG2020 priors, and thus, there are more differences in priors between COCCON v1 and v11.2 OCO-2/v11 OCO-3. An exhaustive list of the differences between the TCCON GGG2020 and the v11.2 OCO-2/v11 OCO-3 priors is provided in Section 4 of Laughner et al. (2023).

3. Coincidence Criteria

This section defines the coincidence criteria used in comparing the X_{CO_2} retrievals from OCO-2/3 against the corresponding coincident COCCON data. Earlier studies, such as Wunch et al. (2017), used a 5° × 10° latitude-longitude box as the spatial coincidence requirement to compare the v7 OCO-2 and GGG2014 TCCON measurements. However, a smaller spatial requirement is used in this study, as the OCO-2 data are available for a longer duration, consistent with Das et al. (2025), who used this criterion for v11.1 OCO-2 versus GGG2020 TCCON comparisons. The OCO-2 versus COCCON comparisons are presented for the OCO-2 land nadir/glint, ocean glint, and target modes. OCO-3 results are shown in the land nadir/glint, ocean glint, target, and SAM modes against COCCON.

Table 1 lists the spatial coincidence criteria used for collocating the OCO-2/3 data around the COCCON site in the land nadir/glint and ocean glint modes. Typically, a coincidence box of 2.5° latitude (±1.25°) and 5° longitude (±2.5°) centered on the COCCON site is treated as suitable, with all OCO-2/3 soundings falling within this area considered spatially coincident. The seven Mexico City sites–Altzomoni, Amec, Boxo, Cuat, Tecamac, Unam, and Vallejo use smaller ±1° × ±1° boxes (Sha et al., 2025). Most of the OCO-2 nadir and glint tracks are located significantly far outside Mexico City, while the COCCON sites are located within or in close proximity to Mexico City. Thus, while the EM27/SUN instruments capture the urban X_{CO_2} enhancements, OCO-2 captures a combination of the urban and (lower) background X_{CO_2}, typically resulting in negative difference values. Thus, the smaller spatial coincidence criteria eliminate a large fraction of the background X_{CO_2} inclusion but also reduce the number of coincidences over these sites. Similarly, for Beijing, Xianghe, Seoul, and Tsukuba, smaller ±0.25° × ±0.25° coincidence boxes are used to reduce collocation errors and the impact of urban versus rural gradients. The temporal collocation criterion treats the median COCCON data within ±1 hr of the OCO-2/3 overpass time as coincident. Furthermore, a minimum of 100 good-quality OCO-2/3 soundings per overpass and at least 15 good-quality COCCON (or TCCON) soundings within the temporal coincidence window are required,

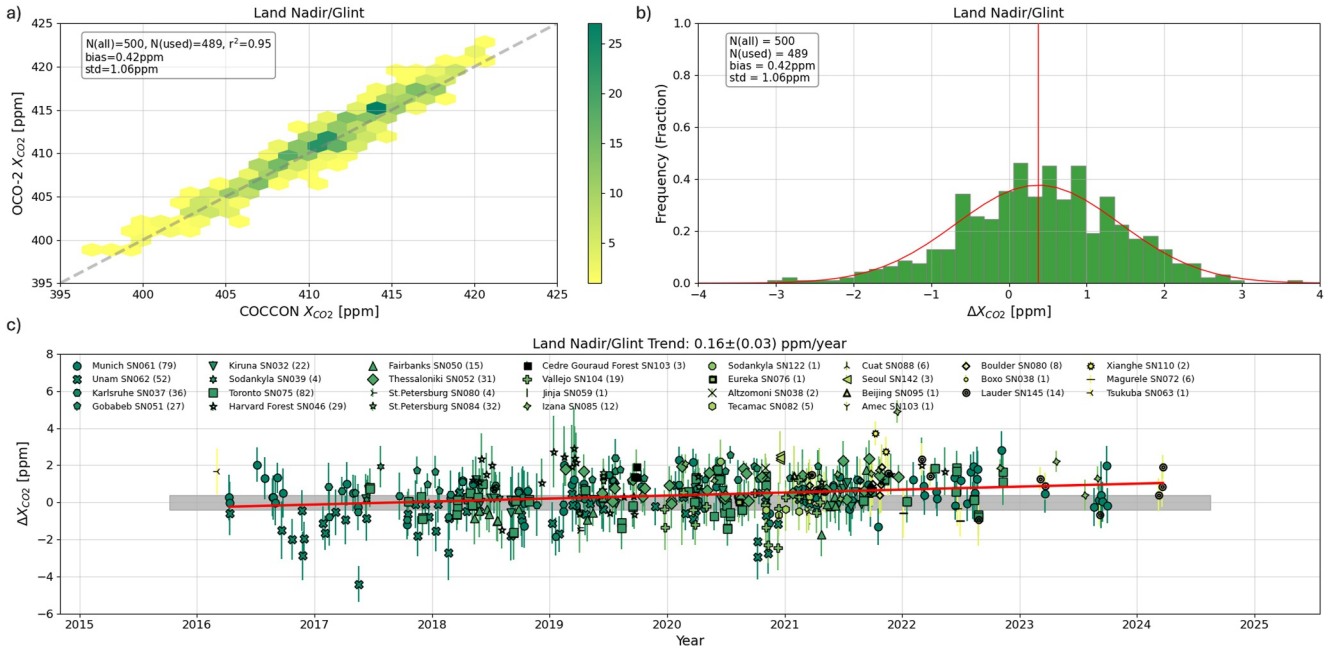

Figure 4. v11.2 OCO-2 Land Nadir/Glint mode–(a) The relation between each OCO-2 land nadir/glint mode observation's median value and the median value of the corresponding coincident COCCON data, recorded within ±1 hr of the OCO-2 overpass. The one-to-one line is indicated by the dashed gray line. The number of coincident data points between OCO-2 and COCCON is indicated by "*N*(all)" and those used for calculating the statistics are indicated by "*N*(used)," the coefficient of determination is represented by "r^2," the difference is represented by "bias," and the standard deviation is indicated by "std." The *x* and *y* axes represent the X_{CO_2} data values in parts per million (ppm) for COCCON and OCO-2, respectively. Data are plotted as a "Hexbin plot," where the color of each hexagonal bin indicates the number of points in it. (b) The histogram provides the distribution of ΔX_{CO_2} (OCO-2 minus COCCON). The *x*-axis shows the value of the difference and the *y*-axis indicates the fraction of observations. (c) The time-series of ΔX_{CO_2}. The markers indicate the different COCCON sites for which coincident OCO-2 data are available. The numbers within the parentheses indicate the *N* (total number of coincidences) value for the corresponding COCCON station. The error bars indicate the standard deviation of ΔX_{CO_2}. The solid red line indicates the time trend in ppm/year. The gray shaded area represents the ±0.4 ppm uncertainty margin.

consistent with Das et al. (2025). The OCO-2 and OCO-3 target mode and the OCO-3 SAM mode measurements are exempt from the spatial coincidence and the minimum 100 good-quality soundings per overpass requirements, as the observations are taken exactly over the COCCON (and TCCON) locations, with minimal collocation error. These coincidence requirements also apply to the OCO-2/3 versus TCCON comparisons shown in Supporting Information S1.

Rodgers and Connor (2003), Connor et al. (2008), Wunch, Wennberg, et al. (2011), and Nguyen and Hobbs (2020) described the need for computing comparative retrievals about a common a priori and the need to apply an averaging kernel correction. It is important to apply averaging kernels to adjust the X_{CO_2} values, as the COCCON and OCO-2/3 X_{CO_2} retrievals were computed using different a priori profiles. Following Wunch, Toon, et al. (2011), an averaging kernel correction was applied for all the COCCON data used in this analysis, using the OCO-2/3 averaging kernels to convolve the COCCON X_{CO_2} values (which are typically small) with the OCO-2/3 column averaging before making comparisons to OCO-2/3 X_{CO_2}.

4. OCO-2 and OCO-3 Versus COCCON v1

4.1. Evaluating OCO-2 Against COCCON v1

Figure 4 compares the bias-corrected and quality-filtered OCO-2 X_{CO_2} data against the corresponding coincident COCCON data in the land nadir and glint modes. This figure is an update to Figure 5 in Sha et al. (2025) and uses the latest v11.2 OCO-2 data. While all OCO-2/3 coincidences against COCCON are shown in this study (represented by "Nall"), only sites with three or more coincident data points are used (indicated by "Nused") in calculating the statistics in all OCO-2/3 figures here and in Supporting Information S1.

Note that since the COCCON data have not been validated as extensively as the TCCON data set so far, the term "bias" is more suitable in the context of OCO-2/3 versus TCCON comparisons, but is also used in the OCO-2/3

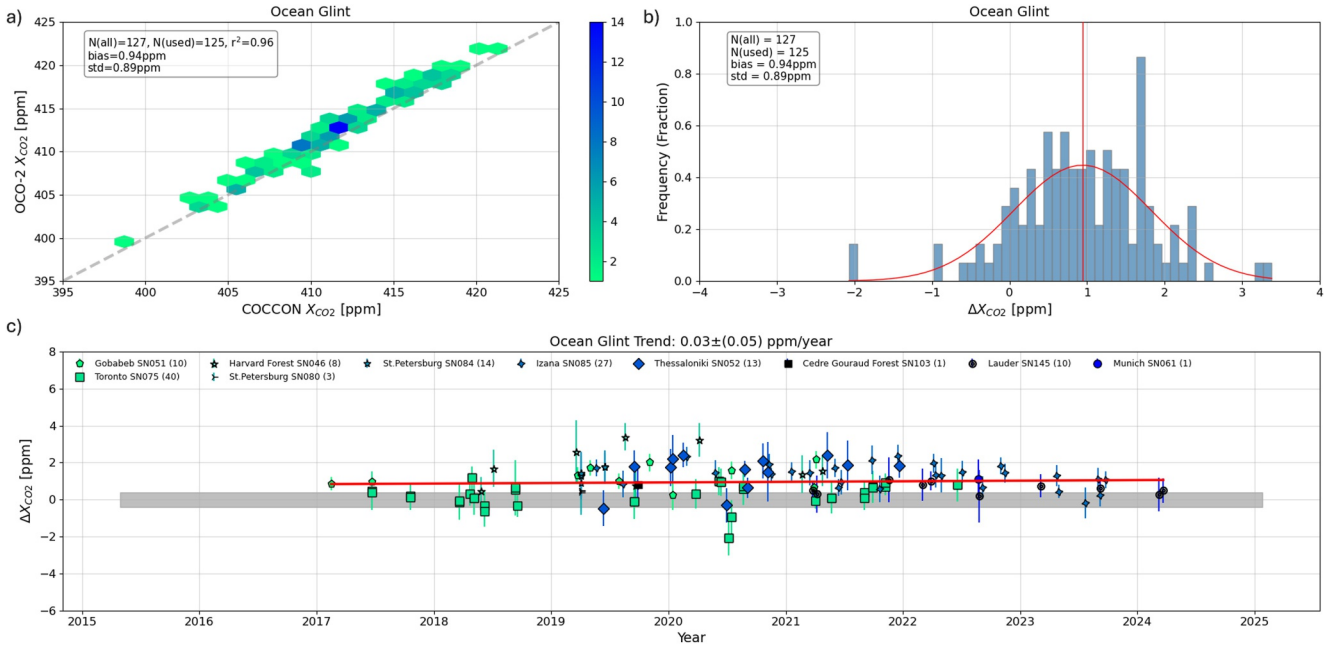

Figure 5. Same as Figure 4, but for v11.2 OCO-2 Ocean Glint mode versus COCCON.

versus COCCON figures for consistency. Due to the limited validation of the COCCON data, this term, in the case of OCO-2/3 versus COCCON comparisons, reflects the mean difference between the ground-based COCCON and the space-based OCO-2/3 measurements.

Panel 4a shows the one-to-one comparison between OCO-2 and COCCON X_{CO_2} data sets during the ±1 hr of the OCO-2 overpass time. In panel 4b, the histogram shows the frequency of the ΔX_{CO_2} (OCO-2 X_{CO_2}–coincident COCCON X_{CO_2}) distribution. Panel 4c shows the time series of the ΔX_{CO_2} values, where a unique marker identifies each COCCON location. In the land nadir/glint mode, there are 500 coincidences ($N_{used} = 489$) between OCO-2 and COCCON, and the globally averaged mean difference is 0.42 ± 1.06 ppm. Negative OCO-2–COCCON differences are typically observed for Unam, Mexico City, due to the reasons discussed in Section 3. The time trends in this study are reported in A ± B ppm/year format. Here, A and B represent the time trend and the statistical uncertainty (standard error) in the time trend, respectively. The time trend, calculated using a linear fit, in the land nadir/glint mode is 0.16 ± 0.03 ppm/year. This trend is mostly driven by a few sites (e.g., Unam and Munich). Due to the complex topography, the sites near Mexico City suggest significant collocation errors. Note that there is no statistically significant time trend between OCO-2 and TCCON land nadir/glint observations (−0.01 ± 0.01 ppm/year, Figure S133 in Supporting Information S1), indicating that this OCO-2/COCCON trend is likely driven by COCCON, such as due to different stations, individual ones of which may be biased, populating different parts of the time record. Given the constraints associated with the COCCON data version discussed in Section 2.3 and the limited COCCON data available for comparison, the aggregated bias-corrected and quality-filtered OCO-2 X_{CO_2} data compare reasonably well against COCCON in the land nadir/glint mode, globally. Several COCCON sites have more than one EM27/SUN instrument, identified by their unique serial numbers (SNs), such as Seoul, Sodankylä, and St. Petersburg. For several sites, the same EM27/SUN instrument is moved to different locations within the same city, that is, the instrument's latitude and longitude change minimally. For such cases, the OCO-2 coincidence box is centered on the varying latitude-longitude of the instrument location, and all data for the same instrument are consolidated and plotted, identified by a unique marker, and labeled as "Location Name" + "SN*xyz*," where "*xyz*" denotes the three-digit SN. Figure S133 in Supporting Information S1 shows the v11.2 OCO-2 versus TCCON GGG2020 results in the land nadir/glint mode.

Figure 5 shows the v11.2 OCO-2 data in the ocean glint mode, compared against the corresponding coincident COCCON data. There are 127 coincidences ($N_{used} = 125$) between OCO-2 and COCCON in this mode, fewer than in other OCO-2 observation modes. This is expected due to the location of fewer COCCON sites near the coastline, in addition to the limited availability of COCCON data. In this mode, the globally averaged mean

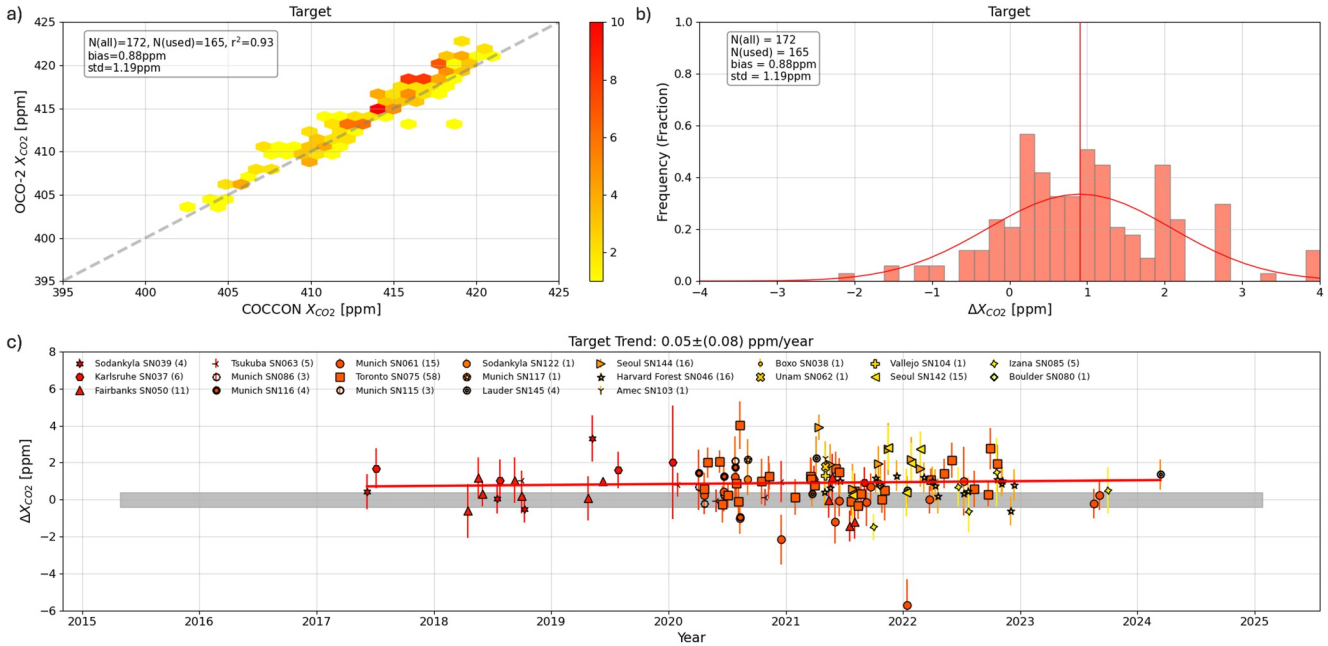

Figure 6. Same as Figure 4, but for v11.2 OCO-2 Target mode versus COCCON.

difference is 0.94 ± 0.89 ppm, with the OCO-2 data being higher than the COCCON data. Figure S134 in Supporting Information S1 shows the v11.2 OCO-2 versus TCCON GGG2020 results in the ocean glint mode, where the r^2 and standard deviation values are comparable to those seen for v11.2 OCO-2 versus COCCON. The high difference seen for v11.2 OCO-2 versus COCCON is not present in the TCCON comparisons. This suggests there may be individually biased COCCON stations, though this is not clear from this analysis alone. Furthermore, the time trend is 0.03 ± 0.05 ppm/year, which is not statistically significant. Note that much of this trend and the difference are driven by sites such as Toronto, Lauder, and Izaña. This is because these are the three sites with the highest number of coincidences and sites for which coincident data against OCO-2 are available after 2021 through the end of the time series. Like in the v11.2 OCO-2 versus TCCON GGG2020 results, the v11.2 OCO-2 versus COCCON results suggest that the standard deviation values for the ocean glint mode are lower than for the land nadir/glint and target mode observations. Unlike the v10, where the ocean glint data were scaled against models, the v11 ocean glint data are scaled using coastline crossings, reducing the overall difference and scatter compared to earlier OCO-2 data versions. Das et al. (2025) (and the corresponding Supporting Information S1) showed v11.1, v10, and v9 OCO-2 comparisons against TCCON. Comparisons between the former v11.1 OCO-2 and v1 COCCON data are shown in Figure S142 of the Supporting Information S1 file of this paper.

Figure 6 shows the v11.2 OCO-2 target mode comparisons against COCCON. The most direct comparison is achieved in this mode due to the high collocation and the minimal collocation error compared to the nadir and glint observation modes. There are 172 coincidences ($N_{\text{used}} = 165$) between OCO-2 and COCCON. The globally averaged OCO-2 mean difference is 0.88 ± 1.19 ppm, which is higher than v11.2 OCO-2 versus TCCON results in the target mode, where the globally averaged OCO-2 bias is −0.01 ± 0.94 ppm, as shown in Figure S135 in Supporting Information S1. The number of coincidences is more evenly distributed between TCCON sites in the OCO-2 versus TCCON comparisons than between COCCON sites in the OCO-2 versus COCCON comparisons. A time trend of 0.05 ± 0.08 ppm/year is seen in the OCO-2 versus COCCON target modes comparisons, which is statistically insignificant. Much of this trend is driven by Toronto, Harvard Forest, and Izaña, three of the few COCCON locations for which coincident COCCON data are available after 2022. The trend is also driven in the opposite direction by Munich (SN061) due to the few days of data impacted by cloud cover, in addition to the occasional small yet concentrated plumes observed by the Munich EM27/SUN that are averaged out over a pixel by OCO-2. Note that the Alps are located ∼50 km south of central Munich, presenting a complex terrain for satellite retrievals. Given the limited COCCON data available and the limited number of coincidences, the

10.1029/2025EA004646

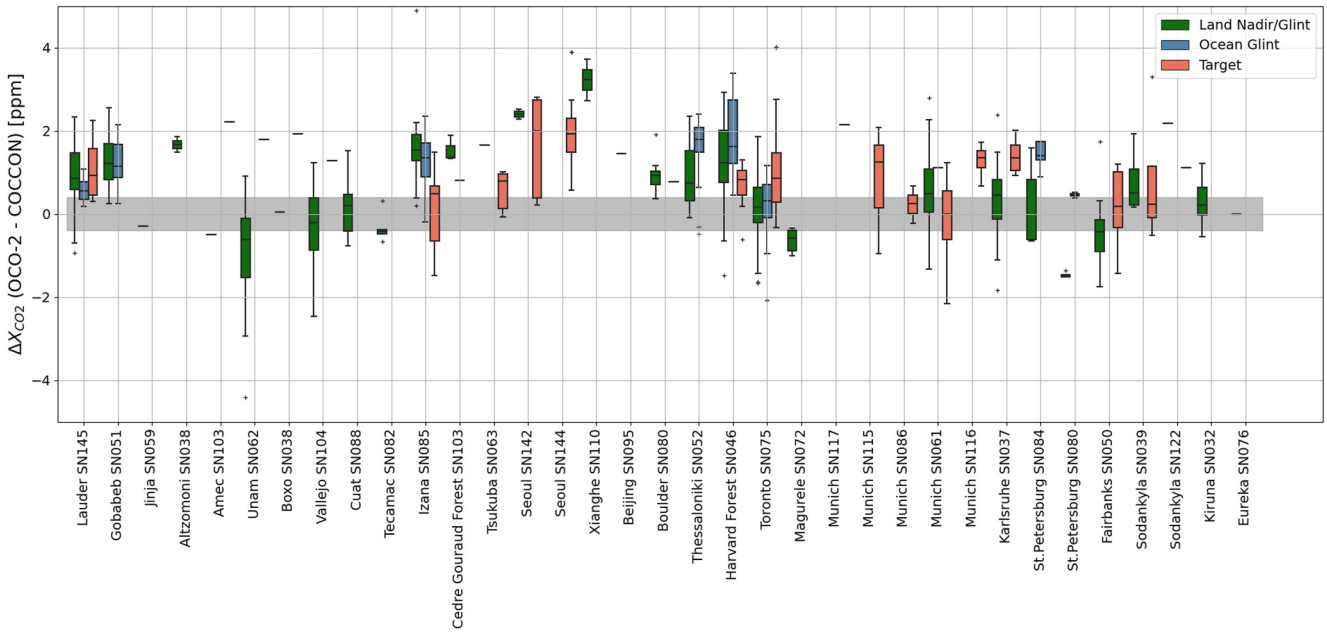

Figure 7. The observation mode-separated site-to-site differences between the v11.2 OCO-2 data and the coincident COCCON data. The bottom and top edges of the boxes indicate the 25 and 75 percentile limits, respectively. The whiskers show the full range of the data excluding outliers, and the outliers are shown by plus ("+") symbols. The gray shaded area represents the ±0.4 ppm uncertainty margin. Note that for sites that have a linear instead of box and whiskers, there is only one overpass.

aggregated bias-corrected and quality-filtered v11.2 OCO-2 X_{CO_2} data compare reasonably well against the corresponding coincident COCCON measurements in the target mode.

The site-to-site differences are shown in Figure 7, where the COCCON sites are plotted on the *x*-axis, ordered by latitude from degrees South on the far left to degrees North on the far right. The EM27/SUN instrument's SN is appended at the end of the site name. For some sites, more than one EM27/SUN instrument is placed at different locations in the same city. Some examples are Seoul SN142 and Seoul SN144, St. Petersburg SN080 and St. Petersburg SN084, and Sodankylä SN039 and Sodankylä SN122. Each instrument has a different number of coincident measurements with the OCO-2 data. Typically, the instruments with more coincidences with OCO-2 for the same site show better agreement across the different observation modes. Figure S136 in Supporting Information S1 shows a plot similar to Figure 7, but for v11.2 OCO-2 versus TCCON. Due to limited coincident data in the ocean glint mode, the improvements, indicated by the reduced difference and scatter compared to earlier OCO-2 data versions (Figure S142 in Supporting Information S1), are most prominent for sites with $N \geq 8$ (e.g., Gobabeb, Thessaloniki, Izaña, Harvard Forest, and Toronto). The most significant improvements in the target mode are seen for the high-latitude sites due to the new DEM.

4.2. Evaluating OCO-3 Against COCCON v1

Figure 8 compares the bias-corrected and quality-filtered OCO-3 X_{CO_2} data against the coincident COCCON data in the land nadir/glint mode. The statistical parameters shown in Figure 8 are akin to those in Figure 4. Panel 8a shows the one-to-one comparison between OCO-3 and COCCON X_{CO_2} data sets during the ±1 hr of the OCO-3 overpass time. The histogram in panel 8b shows the Gaussian distribution of the differences between OCO-3 and the corresponding coincident COCCON data sets (ΔX_{CO_2}). In the land nadir/glint mode, $N_{all} = 199$ ($N_{used} = 191$), and the globally averaged difference value is 0.65 ± 1.06 ppm. The v11 OCO-3 versus TCCON GGG2020 results shown in Figure S137 in Supporting Information S1 for the land nadir/glint mode suggest that OCO-3 data show better agreement with TCCON, compared to COCCON, which is partly attributable to the larger number of coincidences between OCO-3 and TCCON than COCCON. Comparisons between COCCON and the preceding v10.4 OCO-3 (Park et al., 2024) in the land nadir/glint, ocean glint, target, and SAM modes are shown in the Supporting Information S1 (Figure S143). The results suggest comparable/improved statistics, possibly attributable to the v11 OCO-3 algorithm and calibration improvements listed in Section 2.2. The updated DEM improves the retrievals at high latitudes, and the updated land bias correction improves the overall differences in the

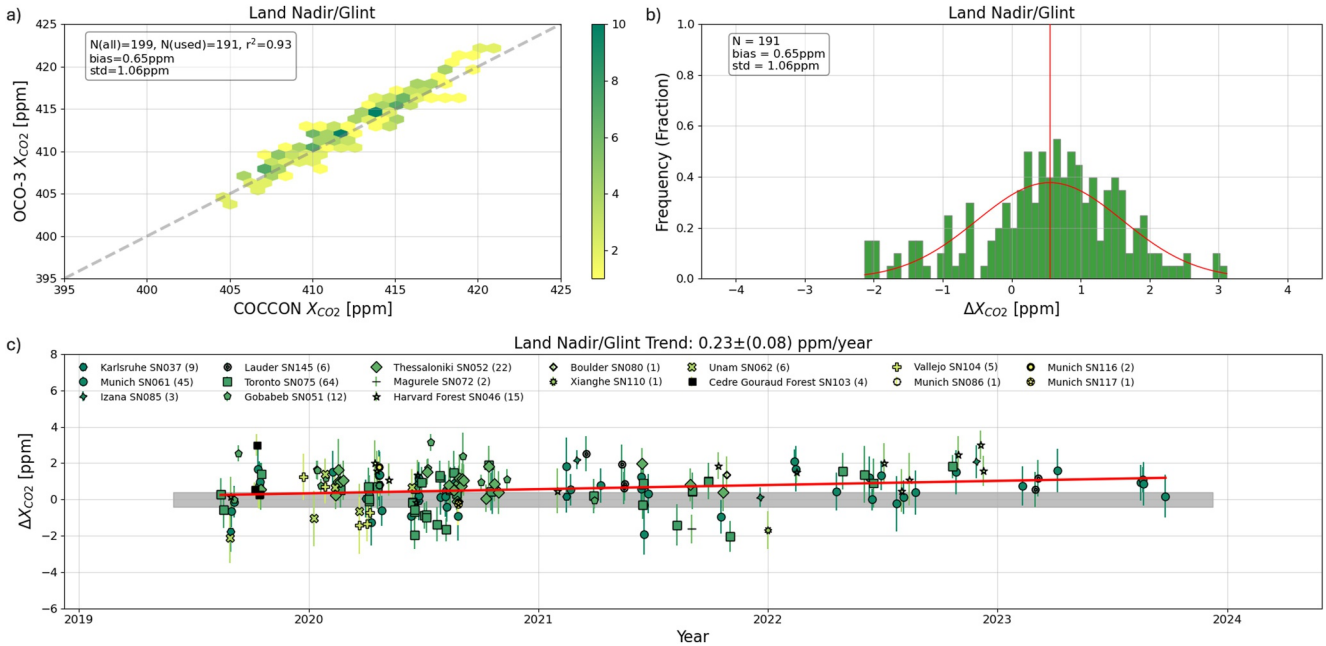

Figure 8. v11 OCO-3 Land Nadir/Glint mode–(a) The relation between each OCO-3 land nadir/glint mode observation's median value and the median value of the corresponding coincident COCCON data, recorded within ±1 hr of the OCO-3 overpass. The one-to-one line is indicated by the dashed gray line. The number of coincident data points between OCO-3 and COCCON is indicated by "*N*(all)" and those used for calculating the statistics are indicated by "*N*(used)," the coefficient of determination is represented by "r^2," the difference is represented by "bias," and the standard deviation is indicated by "std." The *x* and *y* axes represent the X_{CO_2} data values in parts per million (ppm) for COCCON and OCO-3, respectively. Data are plotted as a "Hexbin plot," where the color of each hexagonal bin indicates the number of points in it. (b) The histogram provides the distribution of ΔX_{CO_2} (OCO-3 minus COCCON). The *x*-axis shows the value of the difference and the *y*-axis indicates the fraction of observations. (c) The time-series of ΔX_{CO_2}. The markers indicate the different COCCON sites for which coincident OCO-3 data are available. The numbers within the parentheses indicate the *N* (total number of coincidences) value for the corresponding COCCON station. The error bars indicate the standard deviation of ΔX_{CO_2}. The solid red line indicates the time trend in ppm/year. The gray shaded area represents the ±0.4 ppm uncertainty margin.

land nadir/glint mode. The time-trend is 0.23 ± 0.08 ppm/year, primarily driven by four urban COCCON sites–Thessaloniki, Toronto, Harvard Forest, and Munich. Since COCCON data coincident with OCO-3 are available only for Toronto, Harvard Forest, Munich (SN061), and Lauder after 2022, these sites drive the trend 2022 onwards. As described for Figure 4, for sites with more than one EM27/SUN instrument, the instrument is identified by its unique SN appended after the site name and a unique marker.

Figure 9 shows the v11 OCO-3 versus COCCON results for the ocean glint observations. This has been plotted akin to Figure 5. However, there are very few coincidences between OCO-3 and COCCON in this mode, and they are from Izaña (12 coincidences), Gobabeb (2 coincidences), and Lauder (1 coincidence). The limited coincidences lead to high globally averaged difference values of 0.95 ± 0.47 ppm. Figure S138 in Supporting Information S1 shows the ocean glint mode comparisons between v11 OCO-3 and TCCON. The results indicate a total of 22 coincidences, with reduced bias values, overall, but a higher standard deviation. The improvements to the v11 OCO-3 ocean glint data are discussed in Section 2.2. The time-trend for this mode for OCO-3 versus COCCON is insignificant with a value of −0.13 ± 0.11 ppm/year. Overall, the low number of coincidences between OCO-3 and COCCON increases the uncertainty of the results in the ocean glint mode. With an expanding COCCON data set, improved and robust OCO-3 versus COCCON ocean glint difference estimates will be pertinent to future work.

Figure 10 shows the v11 OCO-3 versus COCCON comparisons for the target mode. For $N_{all} = 94$ ($N_{used} = 90$) between the two data sets in this mode, with a relatively even distribution of coincidences between all COCCON sites until 2022. Given the limited COCCON data available, coincident observations against OCO-3 are present only for Izaña and Lauder 2022 onwards. The globally averaged OCO-3 difference against COCCON is 0.67 ± 1.09 ppm. This is higher than the v11 OCO-3 versus TCCON comparisons, shown in Figure S139 in Supporting Information S1, with a globally averaged difference of 0.16 ± 1.08 ppm with 515 coincidences. The v11 OCO-3 versus COCCON results show a time trend of 0.19 ± 0.10 ppm/year. In the SAM mode, shown in

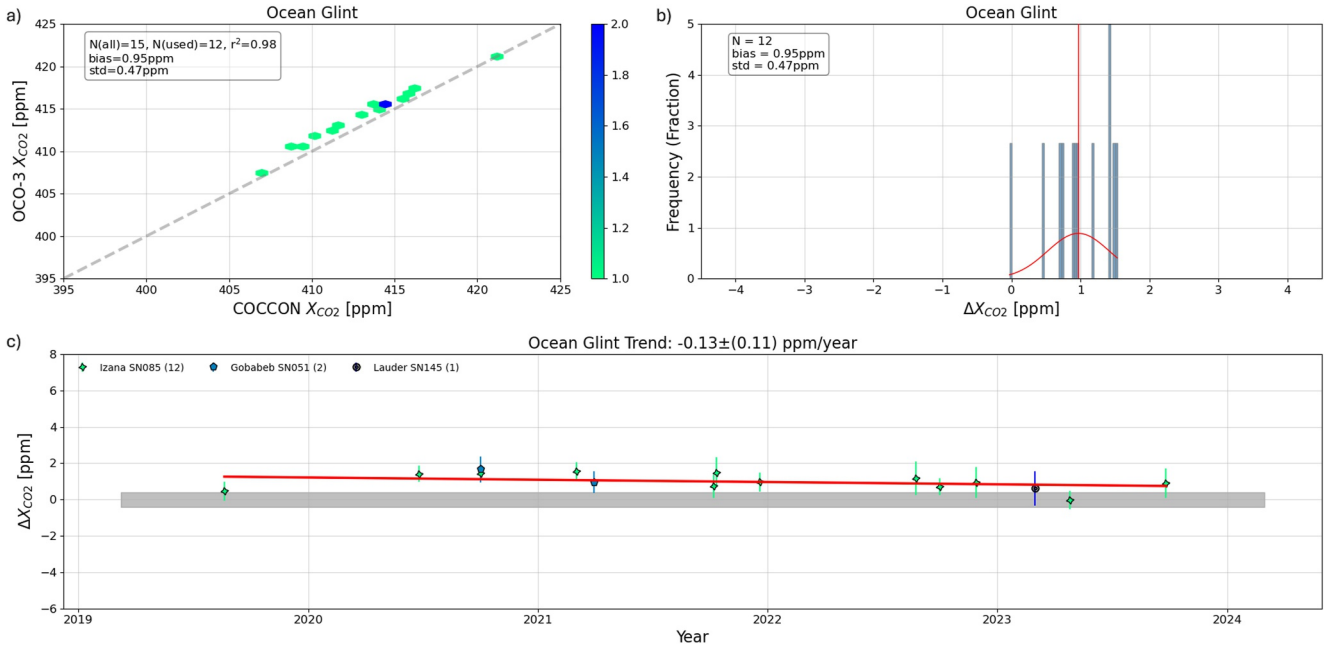

Figure 9. Same as Figure 8, but for v11 OCO-3 Ocean Glint mode versus COCCON.

Figure 11, the globally averaged bias is 0.96 ± 1.18 ppm for the v11 OCO-3 versus COCCON comparison, for $N_{all} = 328$ ($N_{used} = 321$). A relatively lower bias value of 0.25 ± 1.14 ppm was reported for the v11 OCO-3 versus TCCON, shown in Figure S140 in Supporting Information S1, for a comparable number of coincidences. The time trends for OCO-3 versus TCCON and OCO-3 versus COCCON are 0.03 ± 0.06 ppm/year and 0.29 ± 0.08 ppm/year, respectively. Despite the comparable number of coincidences against OCO-3, a relatively small time-trend against TCCON than COCCON is primarily due to the (relatively) even distribution of coincidences amongst TCCON sites. The OCO-3 versus COCCON biases are largely driven by Unam, Vallejo, Munich (SN061), and Toronto, which are urban sites with a likelihood of significant collocation errors.

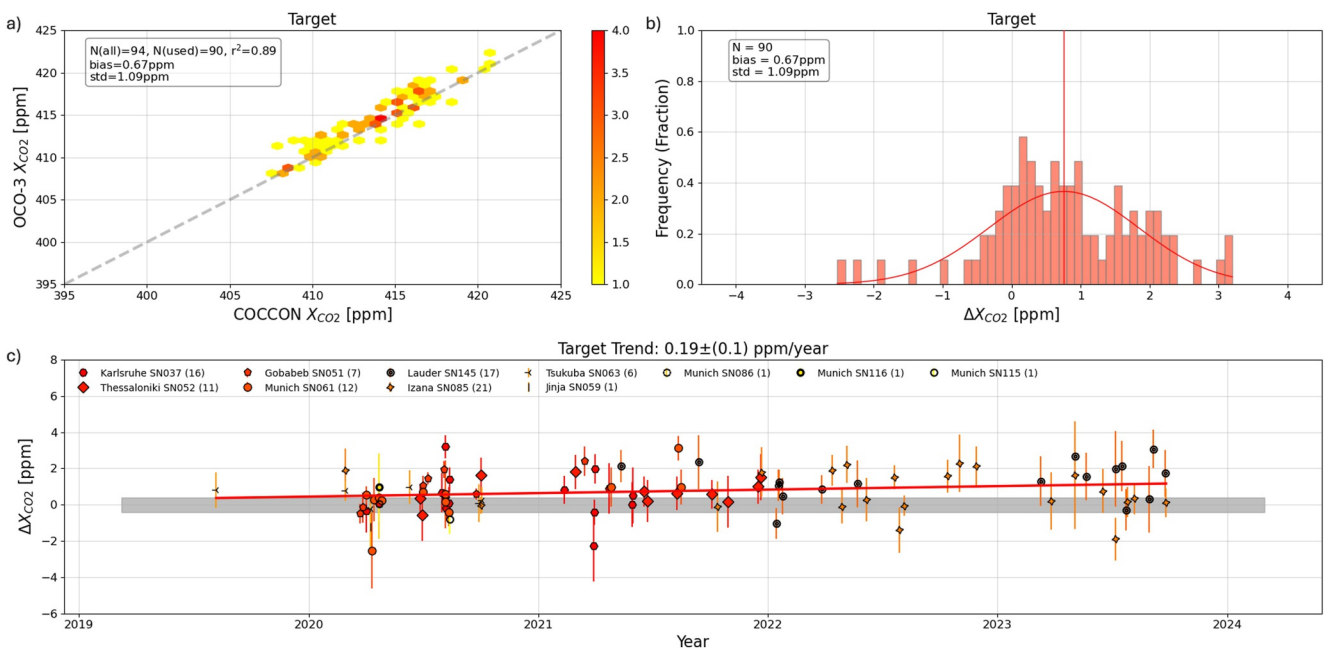

Figure 10. Same as Figure 8, but for v11 OCO-3 Target mode versus COCCON.

10.1029/2025EA004646

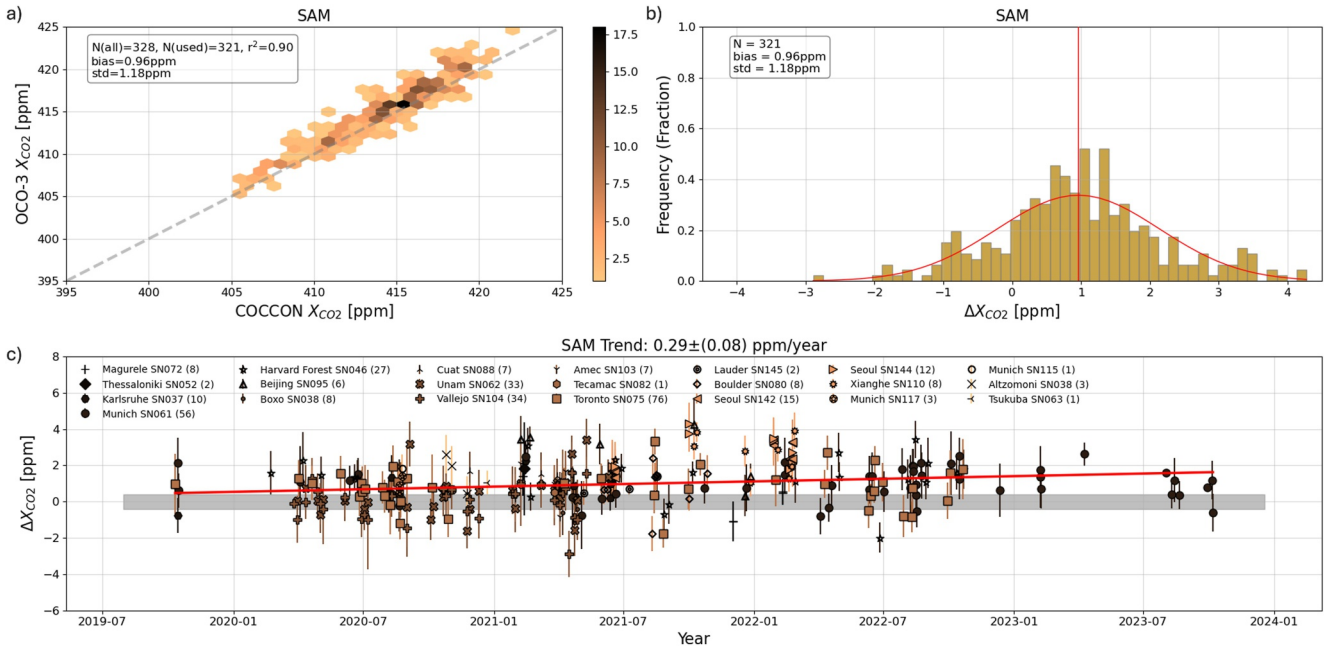

Figure 11. Same as Figure 8, but for v11 OCO-3 SAM mode versus COCCON.

Overall, across all observation modes, OCO-3 shows high difference values against COCCON. The limited number of coincidences, their uneven distribution amongst the various COCCON sites, and the low number of coincidences between OCO-3 and COCCON in the ocean glint mode may contribute to the high global bias values overall. Additionally, due to the reasons mentioned in Section 2.3, the use of the COCCON data processed using PROFFAST v1 introduces some uncertainties that have been mitigated in the latest PROFFAST version, with the caveat that data processed using the latest PROFFAST version are available only for very few COCCON sites. The expanding COCCON data set and the availability of COCCON data processed using the latest PROFFAST version for all sites suggest the possibility of reduced difference values in future comparisons, when all COCCON data are consistently available as v2.4. Overall, considering the limitations and uncertainties, the aggregated bias-corrected and quality-filtered OCO-3 X_{CO_2} data compare reasonably well to coincident COCCON data in the land nadir/glint, target, and SAM modes.

Figure 12 shows the site-to-site differences between v11 OCO-3 and COCCON and is plotted similarly to Figure 7. The sites, listed on the *x*-axis, have been ordered by latitude and plotted from degrees South (far left) to degrees North (far right). The gray-shaded region indicates the ±0.4 ppm uncertainty in the COCCON values (Frey et al., 2019). Similar to the v11.2 OCO-2 versus COCCON results, the v11 OCO-3 versus COCCON results show the best agreement for the land nadir/glint mode. The improved agreement, with a higher number of coincidences, is also seen in the target mode compared to v10.4 OCO-3 due to the updated Global Scaling Factor. In the SAM mode, high differences are seen for Seoul (both EM27/SUNs), Beijing, and Xianghe. High difference values for Xianghe have been observed for v11.2 OCO-2 versus TCCON and COCCON and v11 OCO-3 versus TCCON (Figure S141 in Supporting Information S1), alongside what is observed for v11 OCO-3 versus COCCON in Figure 12. The Xianghe TCCON and COCCON sites are sandwiched between two major urban cities–Beijing and Tianjin, which impact the observations made over Xianghe. Most ocean glint data for Xianghe appear to be made in the Bay of Tianjin, which is several hundred kilometers away from the TCCON/COCCON site, and are possibly impacted by local emissions and point emitters. In Figure S141 in Supporting Information S1, the v11 OCO-3 versus TCCON GGG2020 results suggest significant site-to-site improvements compared to v10.4 OCO-3 versus TCCON GGG2020. Better agreement between v11 OCO-3 and TCCON than COCCON is primarily due to the higher number of coincidences with TCCON across all modes and the role of TCCON in OCO-3 in the bias-correction process.

Table 2 consolidates the global comparisons between the OCO-2/3 data sets against v1 COCCON. The results are separated by observation mode. In the land nadir/glint, ocean glint, and target modes, OCO-2 shows global

10.1029/2025EA004646

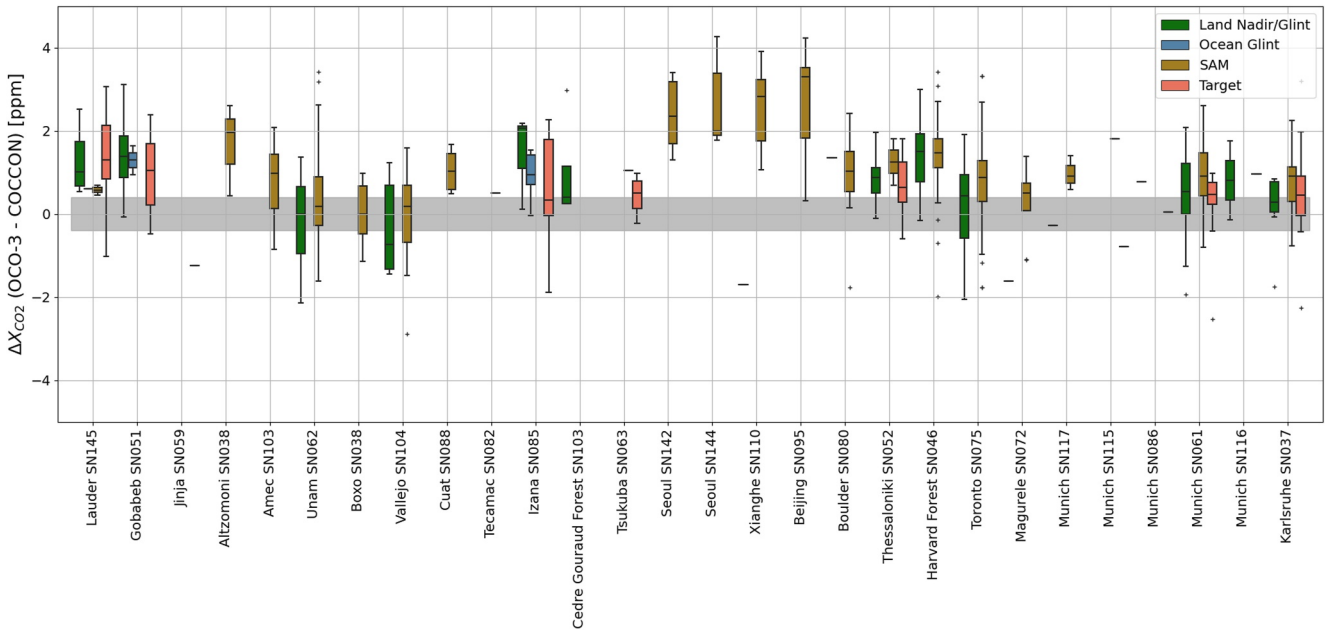

Figure 12. The observation mode-separated site-to-site differences between the v11 OCO-3 data and the coincident COCCON data. The bottom and top edges of the boxes indicate the 25 and 75 percentile limits, respectively. The whiskers show the full range of the data excluding outliers, and the outliers are shown by plus ("+") symbols. The gray shaded area represents the ±0.4 ppm uncertainty margin. Note that for sites that have a linear instead of box and whiskers, there is only one overpass.

mean-difference values of 0.42 ± 1.06 ppm, 0.94 ± 0.89 ppm, and 0.88 ± 1.19 ppm, respectively. In the land nadir/glint, ocean glint, target, and SAM modes, OCO-3 shows global mean-difference values of 0.65 ± 1.06 ppm, 0.95 ± 0.47 ppm, 0.67 ± 1.09 ppm, and 0.96 ± 1.18 ppm, respectively.

4.3. Mexico City Sites

Sections 4.1 and 4.2 showed global comparisons between v1 COCCON X_{CO_2} retrievals against temporally and spatially coincident OCO-2 and OCO-3 X_{CO_2} data, respectively. Figure 4 shows that coincident Mexico City site measurements were typically biased higher than OCO-2, as OCO-2 measurements often include both urban and background CO_2 concentrations, while the EM27/SUNs at the Mexico City sites primarily measured urban CO_2 concentrations. This is also true for the OCO-3 versus v1 COCCON global comparison results shown in Figure 8. EM27/SUN measurements at seven Mexico City sites (Che et al., 2024), namely Amec (SN103), Altzomoni (SN038), Boxo (SN038), Cuat (SN088), Tecamac (SN013), Unam (SN062), and Vallejo (SN104), have been

Table 2
OCO-2 Land Nadir/Glint, Ocean Glint, and Target Mode Statistics, and OCO-3 Land Nadir/Glint, Ocean Glint, Target, and SAM Mode Statistics for Data Filtered Using the xco2_quality_flag = 0

Global analysis					
Satellite data set	Observation mode	Difference (ppm)	Std dev (ppm)	R^2	N_{all}/N_{used}
v11.2 OCO-2	Land Nadir/Glint	0.42	1.06	0.95	500/489
v11.2 OCO-2	Ocean Glint	0.94	0.89	0.96	127/125
v11.2 OCO-2	Target	0.88	1.19	0.93	172/165
v11 OCO-3	Land Nadir/Glint	0.65	1.06	0.93	199/191
v11 OCO-3	Ocean Glint	0.95	0.47	0.98	15/12
v11 OCO-3	Target	0.67	1.09	0.89	94/90
v11 OCO-3	SAM	0.96	1.18	0.90	328/321

Note. The difference (OCO-2/OCO-3 − COCCON), Standard deviation (Std Dev), R^2, and the number of coincidences (N_{all}/N_{used}) are listed below for global comparisons between OCO-2/OCO-3 and v1 COCCON.

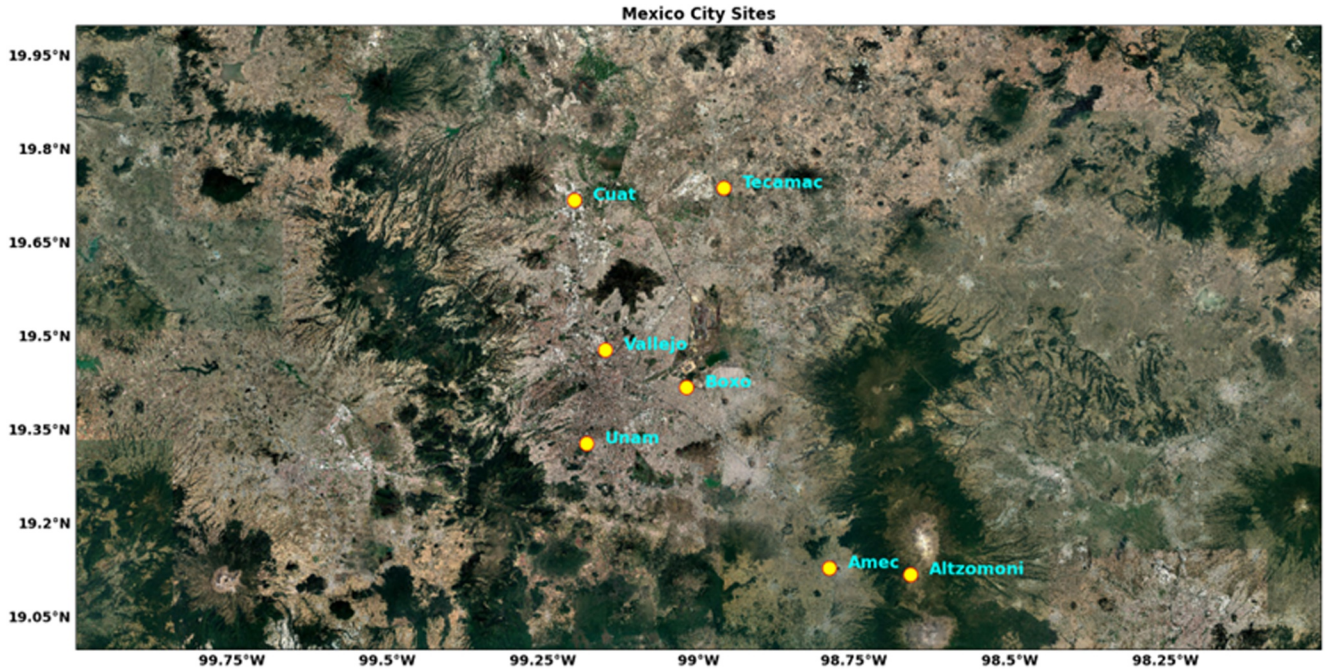

Figure 13. Map of all Mexico City EM27/SUN locations; yellow circles identify the sites.

used in this analysis. Due to a significant number of collocations between some of these sites with OCO-2 and OCO-3, evaluating them separately against the satellite data sets is pertinent, in addition to the independent global analysis. Figure 13 shows a map of the Mexico City sites, with the yellow circles indicating the EM27/SUN locations. The time series for each EM27/SUN is shown in Supporting Information S1 file (Figures S13–S18).

Figure 14 shows the one-to-one relationship between v11.2 OCO-2 and v1 COCCON in the land nadir/glint mode for all Mexico City sites, where the median OCO-2 value is compared against the corresponding coincident COCCON data that qualify the spatial and temporal coincidence requirements. In the OCO-2 land nadir/glint mode, coincident COCCON measurements are available for five of the seven Mexico City sites–Unam, Valleho, Altzomoni, Tecamac, and Boxo. A total of 86 coincidences ($N_{used} = 82$) are available and indicate an average bias value of –0.46 ± 1.05 ppm. As discussed in Section 4.1, the OCO-2 land nadir/glint tracks lie away from the EM27/SUN location and thus capture a combination of urban and background CO_2, while the EM27/SUNs typically measure urban emissions, resulting in a noticeable negative bias, where OCO-2 reports lower X_{CO_2} values than the coincident COCCON data. Equivalent comparisons for the OCO-2 target mode are shown in Figure S19 in Supporting Information S1, but do not have statistics shown due to insufficient coincidences.

Figures S20 and S21 in Supporting Information S1 are plotted similarly to Figure 14, but for v11, OCO-3 versus COCCON in the land nadir/glint and SAM modes, respectively. The difference values in these modes are –0.66 ± 1.21 ppm ($N_{all} = N_{used} = 11$) and 0.37 ± 1.04 ppm ($N_{all} = 93/N_{used} = 92$), respectively. The high and negative bias observed in the OCO-3 land nadir/glint mode data against COCCON is due to reasons similar to those described for OCO-2 versus COCCON. The SAM measurements, unlike the land nadir/glint measurements, primarily capture urban enhancements and, therefore, show smaller absolute bias values against COCCON.

5. OCO-2 and OCO-3 Versus v2.x PROFFAST

While this study used the v1 PROFFAST processed COCCON data for global comparisons due to reasons discussed earlier, limited COCCON sites across the globe have their data available, processed using PROFFAST v2.x (v2.x COCCON data, hereafter). This section evaluates the OCO-2 and OCO-3 X_{CO_2} data against coincident v2 COCCON measurements. Note that each site with v2 COCCON data was processed independently by the respective institution. Each institution used its own subversion of PROFFAST v2. Thus, all v2 COCCON data are available in inconsistent v2 sub-versions. For example, the COCCON data for Thessaloniki is processed using PROFFAST v2, Munich and Seoul are processed using PROFFAST v2.2, and Harvard Forest and Lauder are

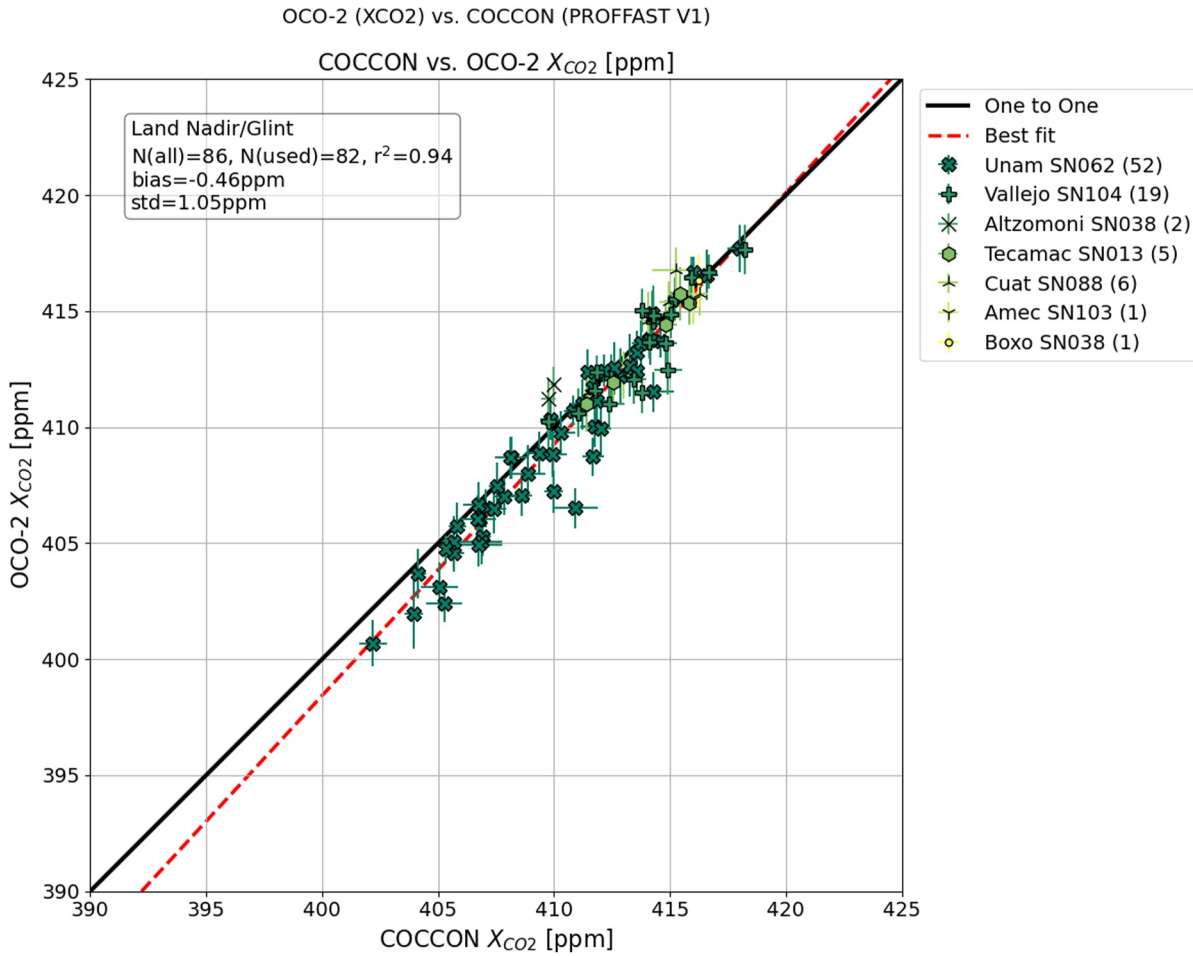

Figure 14. One-to-one plot indicating the relation between each v11.2 OCO-2 land nadir/glint-mode data's median value for all Mexico City sites and the corresponding coincident COCCON (PROFFAST v1) data, recorded within ±1 hr of the OCO-2 overpass. The solid black line is the one-to-one line and the dashed red line indicates the best fit (linear fit). The numbers within the parentheses next to the COCCON site names indicate the number of coincident observations between OCO-2 and COCCON. The error bars indicate the standard deviation about the median.

processed using PROFFAST v2.4. The PROFFAST v2 retrieval included forward model updates and spectroscopic improvements over v1. In v2.1, incorporated core spectroscopic updates introduced in v2. The v2.2 PROFFAST version worked on retrieval accuracy, and v2.3 (Feld et al., 2024) focused on improved calibration to accommodate an updated solar line list. The latest v2.4 PROFFAST includes calibration refinements (particularly regarding the Airmass Dependent Correction Factors (ADCFs) and Airmass Independent Correction Factors (AICFs) to match TCCON data and eliminate potential offsets) and implemented an empirical H_2O correction factor. Detailed information regarding each PROFFAST sub-version can be found on the KIT webpage: https://www.coccon.kit.edu/71.php.

The time-series and description of each EM27/SUN at locations with v2.x COCCON data are explained in Supporting Information S1. Figure 15 shows the one-to-one relationship between v11.2 OCO-2 and v2.x COCCON in the land nadir/glint mode, where the median OCO-2 value is compared against the corresponding coincident COCCON data that qualify the spatial and temporal coincidence requirements. Note that for Seoul, the "L#" value at the end of the site name indicates the location number since the EM27/SUN measured at more than one location within Seoul. Due to the difference in the data periods available for v1 and v2.x COCCON, more coincidences are available for v11.2 OCO-2 versus v1 COCCON than v2.x COCCON. Table 3 lists the figure number and description of the v11.2 OCO-2/v11 OCO-3 comparisons against v1/v2.x COCCON for sites that have data available in both PROFFAST-processed versions, with the corresponding statistical parameters listed in Table 4.

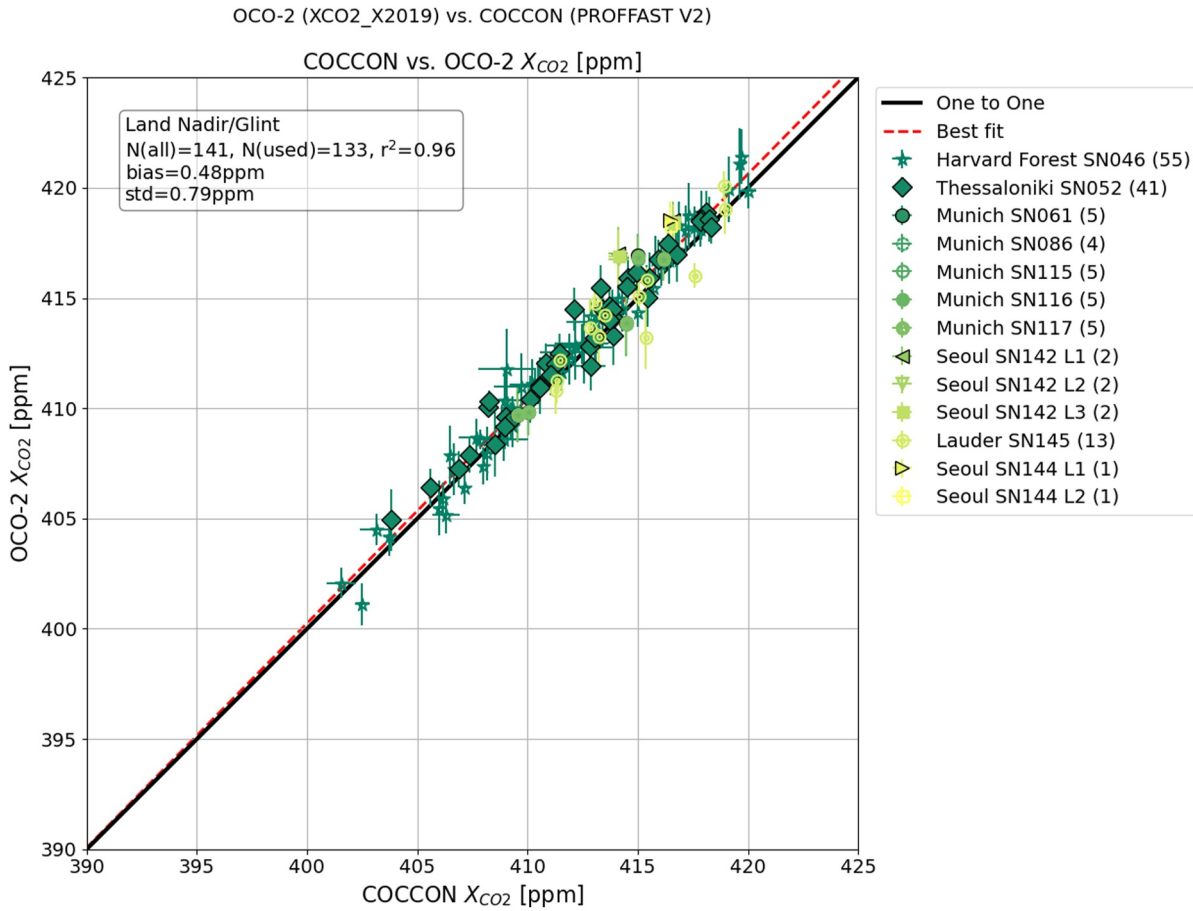

Figure 15. One-to-one plot indicating the relation between each v11.2 OCO-2 land nadir/glint-mode data's median value and the corresponding coincident COCCON (PROFFAST v2.x) data, recorded within ±1 hr of the OCO-2 overpass. The solid black line is the one-to-one line and the dashed red line indicates the best fit (linear fit). The numbers within the parentheses next to the COCCON site names indicate the number of coincident observations between OCO-2 and COCCON. The error bars indicate the standard deviation about the median. The "L#" value at the end of the Seoul COCCON site indicates the location number as the EM27/SUN measured at more than one location within Seoul.

Table 4, similar to Table 2, shows comparisons between OCO-2/3 data sets against v2.x COCCON for selected sites, and between the OCO-2/3 data sets and v1 COCCON for all Mexico City Sites. Table 4 is a subset of Table 2, where the statistical values for the sites with data for both v1 and v2.x COCCON are listed. Against v2.x COCCON, for selected sites where COCCON data are available, OCO-2 shows difference values of 0.48 ± 0.79 ppm, 0.84 ± 0.83 ppm, and 0.77 ± 1.42 ppm in the land nadir/glint, ocean glint, and target modes, respectively. OCO-3 shows difference values of 0.16 ± 0.96 ppm, 0.62 ± 0.92 ppm, and 1.15 ± 1.15 ppm in the land nadir/glint, target, and SAM modes, respectively. The difference values vary by ∼0.08 ppm for OCO-2 and OCO-3 X_{CO_2} data on the X2007 scale (not shown). The difference values for the Mexico City Sites are −0.46 ± 1.05 ppm and −0.66 ± 1.21 ppm in the land nadir/glint mode for OCO-2 and OCO-3, respectively. OCO-3 has a difference value of 0.37 ± 1.04 ppm in the SAM mode against COCCON.

Overall, the v2.x COCCON data set agrees better with OCO-2 and OCO-3 across all observation modes compared to v1 COCCON, with reduced difference values between OCO-2/3 and COCCON due to the improvements in the PROFFAST v2.x, discussed in Section 2.3.

6. Conclusions

The aggregated bias-corrected and quality-filtered (xco2_quality_flag = 0) OCO-2/3 X_{CO_2}retrievals are compared to v1 COCCON data globally, and to v2.x COCCON data for selected COCCON sites. This study

Table 3
Figure Number and Description of the One-to-One Relationship Between v11.2 OCO-2/v11 OCO-3 Versus v1/v2.x COCCON Data Across All Observation Modes for COCCON Sites With Both v1 and v2.x Data Versions Available

Figure Number	Description
Figure 15	One-to-one relationship between v11.2 OCO-2 and v2.x COCCON in the land nadir/glint mode
Figure 16	One-to-one relationship between v11 OCO-3 and v2.x COCCON in the land nadir/glint mode
Figure S33 in Supporting Information S1	Same as Figure 15 v11.2 OCO-2 ocean glint observations versus v2.x COCCON
Figure S34 in Supporting Information S1	Same as Figure 15 v11.2 OCO-2 target mode observations versus v2.x COCCON
Figure S35 in Supporting Information S1	Same as Figure 16, but in the target mode of observation
Figure S36 in Supporting Information S1	Same as Figure 16, but in the SAM mode of observation
Figure S37 in Supporting Information S1	Same as Figure 15 (and for the same COCCON sites) but for v11.2 OCO-2 versus v1 COCCON
Figure S38 in Supporting Information S1	Same as Figure S33 in Supporting Information S1, but for v11.2 OCO-2 versus v1 COCCON
Figure S39 in Supporting Information S1	Same as Figure S34 in Supporting Information S1, but for v11.2 OCO-2 versus v1 COCCON
Figure S40 in Supporting Information S1	Same as Figure 16 but for v11 OCO-3 versus v1 COCCON
Figure S41 in Supporting Information S1	Same as Figure S35 in Supporting Information S1 but for v11 OCO-3 versus v1 COCCON
Figure S42 in Supporting Information S1	Same as Figure S36 in Supporting Information S1 but for v11 OCO-3 versus v1 COCCON

Table 4
OCO-2 Land Nadir/Glint, Ocean Glint, and Target Mode Statistics, and OCO-3 Land Nadir/Glint, Ocean Glint, Target, and SAM Mode Statistics for Data Filtered Using the xco2_quality_flag = 0

OCO-2/OCO-3 versus v1/v2.x COCCON					
Satellite Data set/COCCON version	Observation mode	Difference (ppm)	Std dev (ppm)	R^2	N_{all}/N_{used}
OCO-2/v1	Land Nadir/Glint	0.73	0.88	0.97	156/153
OCO-2/v2.x	Land Nadir/Glint	0.48	0.79	0.96	141/133
OCO-2/v1	Ocean Glint	1.37	0.96	0.94	32/31
OCO-2/v2.x	Ocean Glint	0.84	0.83	0.95	38/38
OCO-2/v1	Target	0.94	1.37	0.85	77/76
OCO-2/v2.x	Target	0.77	1.42	0.88	83/83
OCO-3/v1	Land Nadir/Glint	0.85	0.88	0.95	92/88
OCO-3/v2.x	Land Nadir/Glint	0.16	0.96	0.93	122/122
OCO-3/v1	Target	0.79	1.10	0.85	43/40
OCO-3/v2.x	Target	0.62	0.92	0.93	56/54
OCO-3/v1	SAM	1.41	1.06	0.92	118/113
OCO-3/v2.x	SAM	1.15	1.15	0.94	126/122
Mexico City sites (v1 COCCON data)					
Satellite data set					
v11.2 OCO-2	Land Nadir/Glint	−0.46	1.05	0.94	86/82
v11 OCO-3	Land Nadir/Glint	−0.66	1.21	0.58	11/11
v11 OCO-3	SAM	0.37	1.04	0.81	93/92

Note. The difference (OCO-2/OCO-3 − COCCON), Standard deviation (Std Dev), R^2, and the number of coincidences (N_{all}/N_{used}) are shown for sites with v1 and v2.x COCCON data versus OCO-2/OCO-3, and the Mexico City Sites. For the comparison between OCO-2/3 and COCCON, the satellite data set (v11.2 OCO-2/v11 OCO-3) and COCCON version (v1/v2.x) are listed as "satellite data set/COCCON version."

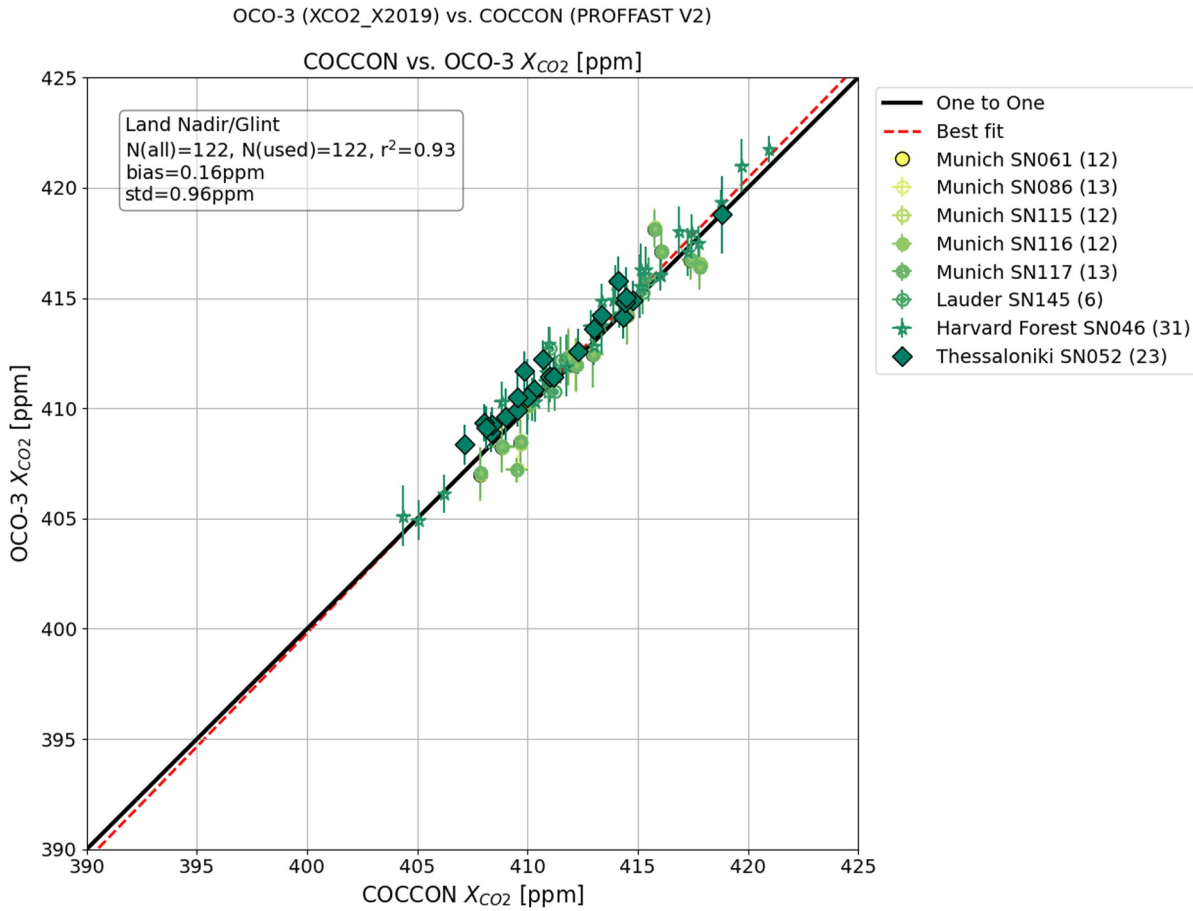

Figure 16. One-to-one plot indicating the relation between each v11 OCO-3 land nadir/glint-mode data's median value and the corresponding coincident COCCON (PROFFAST v2.x) data, recorded within ±1 hr of the OCO-3 overpass. The solid black line is the one-to-one line and the dashed red line indicates the best fit (linear fit). The numbers within the parentheses next to the COCCON site names indicate the number of coincident observations between OCO-3 and COCCON. The error bars indicate the standard deviation about the median.

presents, for the first time, a detailed global comparison between COCCON and the latest v11.2 OCO-2 and v11 OCO-3 data versions.

For OCO-2 compared globally against v1 COCCON, in the land nadir/glint observation mode, the mean difference is 0.42 ± 1.06 ppm with an R^2 value of 0.95. In the ocean glint observation mode, the mean difference is 0.94 ± 0.89 ppm, and the R^2 value is 0.96. The mean difference in the target observation mode is 0.88 ± 1.19 ppm, and the R^2 value is 0.93. Generally, the COCCON data are lower than the collocated OCO-2 observations for all observation modes. The standard deviations are higher for the COCCON comparisons relative to similar TCCON analyses (Das et al., 2025, and Supporting Information S1), which is to be expected given the difference in spectral resolution between the spectrometers used. The R^2 values for the OCO-2/3 versus COCCON comparisons are similar to those seen in the TCCON analysis and suggest that the COCCON data can be useful in the future as the product quality increases.

For OCO-3 X_{CO_2} compared globally against v1 COCCON, the COCCON data values are typically lower across all satellite observation modes. Specifically, for the land nadir/glint observation mode, the mean difference is 0.65 ± 1.06 ppm, with an R^2 value of 0.93. In the case of ocean glint observations, the mean difference is 0.95 ± 0.47 ppm, and the R^2 value is 0.98, but with a relatively small number of comparisons. It is hoped that as more COCCON sites update their data product consistently to v2.4, the number of coincidences with the satellite will increase. The mean difference in the target observation mode is 0.67 ± 1.09 ppm, and the R^2 value is 0.89. In the SAM mode, the mean difference is 0.96 ± 1.18 ppm, and the R^2 value is 0.90. For OCO-2 and OCO-3, the difference values indicate a statistically significant time-dependent trend in the land nadir/glint mode that is not

seen in the TCCON comparisons. This could be attributed to differences in observation site properties between TCCON and COCCON or collocation errors over specific sites. Additionally, the use of an older PROFFAST version for the global comparisons and the limited COCCON data available, which are processed using the latest PROFFAST version, could be affecting the comparisons. Furthermore, it should be noted that the sites with v1 data used in global analysis contain a higher percentage of urban, potentially more polluted locations than the locations of TCCON sites. This could affect the retrievals through the effects of the a priori information in the retrievals. As the COCCON retrievals and calibration evolve, we would expect the COCCON data to become a valuable tool for the evaluation of satellite observations.

TCCON has historically been the gold-standard ground-based validation data set for OCO-2 and OCO-3. Formerly, Wunch et al. (2017) compared v7 OCO-2 against TCCON. Das et al. (2025) updated and expanded upon that validation analysis using OCO-2 v11.1 data. These analyses illustrate the quality of the OCO-2 data products and the utility of the TCCON network as a tool for validating satellite data. As a part of the analysis presented here, we have updated our TCCON comparisons to include the most recent v11.2 OCO-2 data product and provide the first validation result for v11 OCO-3 versus TCCON (Figures S137 through S141 in Supporting Information S1). We included these results for context for the COCCON comparisons, and the OCO-3 versus TCCON comparisons will be the subject of future analysis.

OCO-2/3 compared to v2.x COCCON data for selected sites (where v2.x COCCON measurements are available) suggest better agreement due to the improvements in the PROFFAST v2.x retrieval software, discussed in Section 2.3. The comparisons between COCCON v2.x and the satellites move toward values that are in line with the OCO-2 and OCO-3 comparisons against TCCON. For OCO-2, the difference values against v2.x COCCON in the land nadir/glint, ocean glint, and target observation modes are 0.48 ± 0.79 ppm ($R^2 = 0.96$), 0.84 ± 0.83 ppm ($R^2 = 0.95$), and 0.77 ± 1.42 ppm ($R^2 = 0.88$), respectively. For OCO-3, the difference values against v2.x COCCON in the land nadir/glint, target, and SAM observation modes are 0.16 ± 0.96 ppm ($R^2 = 0.93$), 0.62 ± 0.92 ppm ($R^2 = 0.93$), and 1.15 ± 1.15 ppm ($R^2 = 0.94$), respectively. Mexico City Sites collectively form a large fraction of the total coincidences in the land nadir/glint and SAM modes. For OCO-2 and OCO-3, the difference values against COCCON show values of -0.46 ± 1.05 ppm ($R^2 = 0.94$) and -0.66 ± 1.21 ppm ($R^2 = 0.58$) in the land nadir/glint mode, respectively. OCO-3, in the SAM mode, shows a difference of 0.37 ± 1.04 ppm ($R^2 = 0.81$) against COCCON.

This study provides the first global comparison of satellite estimates of X_{CO_2} to ground-based EM27/SUN observations. The v11.2 OCO-2 and v11 OCO-3 data sets show reasonable agreement with v1 COCCON over all modes, with some comparisons limited by the number of coincidences and other uncertainties. The comparisons in this study suggest that the new and improved v11.2 OCO-2 and v11 OCO-3 X_{CO_2} data versions are robust for use by the scientific community, as has been shown in other studies for previous data versions. The comparisons of the satellite data to the COCCON observations also provide an important data set that includes new locations where TCCON observations are not available. The COCCON measurements, thus, provide additional comparisons that complement the TCCON measurements. Future evolution of the COCCON data set, with the latest data version and calibration, will increase the utility of the EM27/SUN instruments for evaluating satellite data. The fact that many of the EM27/SUN sites are located in urban, often polluted locations, provides new opportunities for regional comparisons and for studying the satellite data in different emission scenarios.

Future efforts to validate satellite observations of greenhouse gases could consider using the TCCON and COCCON data sets in combination to enhance the global coverage. Use of the COCCON data in validation analyses would benefit greatly from a consistent data product, uniformly processed using the latest PROFFAST version, and the continued side-by-side measurements at TCCON sites, to augment the capabilities of TCCON. The limited comparisons to v2.x COCCON data shown in this study suggest that improved global comparisons to the satellite data will be possible when more data are available.

Conflict of Interest

The authors declare no conflicts of interest relevant to this study.

Acknowledgments
Gratitude is expressed to Drs. Michael R. Gunson and Paul O. Wennberg for their feedback on this work. We thank Drs. Jason M. St Clair, Thomas F. Hanisco, and Lesley E. Ott for providing the resources to revise this work, in part, at the NASA Goddard Space Flight Center. This work has been supported by the National Aeronautics and Space Administration. Part of this research was carried out at the Jet Propulsion Laboratory, California Institute of Technology, under contract with the National Aeronautics and Space Administration (80NM0018D0004). Government sponsorship is acknowledged.

The TCCON site at Réunion Island has been operated by the Royal Belgian Institute for Space Aeronomy with financial support since 2014 by the EU project ICOSINIWRE (Grant agreement 313169), the ministerial decree for ICOS (Grant FR/35/IC1 to FR/35/C6), the ESFRI-FED ICOSBE project (Grant EF/211/ICOS-BE), and local activities supported by LACy/UMR8105 and by OSU-R/UMS3365–Université de La Réunion. TCCON sites at Tsukuba, Rikubetsu, and Burgos are supported in part by the GOSAT series project. Burgos is supported in part by the Energy Development Corporation, Philippines. The TCCON Nicosia site has received additional support from the European Union's Horizon 2020 research and innovation programme under Grant agreement 856612 (EMME-CARE) and the Cyprus Government, and by the University of Bremen. The Edwards TCCON station is supported by NASA's Earth Science Division. The Eureka TCCON measurements were made at the Polar Environment Atmospheric Research Laboratory (PEARL) by the Canadian Network for the Detection of Atmospheric Change (CANDAC), primarily supported by the Natural Sciences and Engineering Research Council of Canada, Environment and Climate Change Canada, and the Canadian Space Agency. The Paris TCCON site has received funding from Sorbonne Université, the French research center CNRS, and the French space agency CNES. The Park Falls TCCON site, the TCCON data archive, including data QA/QC, and the development of the ggg2020 retrieval are supported by NASA via 80NSSC22K1066. The Boulder COCCON site was supported by NASA ROSES Grant 80NSSC18K0898 and JPL awards 1669866 and 1615988. The COCCON site at Tsukuba is supported in part by the GOSAT series project and the Environment Research and Technology Development Fund of the ERCA (JPMEERF20252003) funded by the Ministry of the Environment. Drs. Neil Humpage and Robert Parker would like to acknowledge Dr. William Okello and the staff at the National Fisheries Resources Research Institute in Jinja for their

Availability Statement

OCO-2 and OCO-3 Lite files are produced by the NASA OCO-2 and OCO-3 projects, respectively, at the Jet Propulsion Laboratory, California Institute of Technology. Version 11.2 (v11.2) OCO-2 (OCO-2 Science Team, 2014) and version 11 (v11) OCO-3 (OCO-3 Science Team, 2019) Lite files are available from NASA Goddard Earth Science Data and Information Services Center. The v1 COCCON data are available from the COCCON data archive, hosted by the Karlsruhe Institute of Technology (KIT) (https://www.coccon.kit.edu/72.php, last access: 5 May 2026; COCCON Team, 2026). The v1 COCCON data for Beijing and Xianghe used in this study can be publicly accessed (Zhou & Cai, 2026). The Munich v1 and v2.2 data for SN061 are available on the KIT COCCON data archive. The v1 and v2.2 data for all other Munich EM27/SUNs can be publicly accessed (Chen et al., 2026). The complete v2.x COCCON data set is currently being re-processed, and data for individual sites used in this analysis are available on the KIT COCCON data archive. TCCON data are available from the TCCON data archive, hosted by CaltechDATA (https://tccondata.org/, last access: 5 May 2026; TCCON Team, 2026). The references to data from individual TCCON and COCCON sites are listed in Tables S1 and S2 in Supporting Information S1. All analyses were performed using Python 3.9 (https://www.python.org/).

References

Alberti, C., Hase, F., Frey, M., Dubravica, D., Blumenstock, T., Dehn, A., et al. (2022). Improved calibration procedures for the EM27/SUN spectrometers of the COllaborative Carbon Column Observing Network (COCCON). *Atmospheric Measurement Techniques*, *15*(8), 2433–2463. https://doi.org/10.5194/amt-15-2433-2022

Basilio, R. R., Bennett, M. W., Eldering, A., Lawson, P. R., & Rosenberg, R. A. (2019). Orbiting Carbon Observatory-3 (OCO-3), remote sensing from the International Space station (ISS). In *Sensors, systems, and next-generation satellites XXIII* (Vol. 11151, pp. 42–55). https://doi.org/10.1117/12.2534996

Bell, E., O'Dell, C. W., Taylor, T. E., Merrelli, A., Nelson, R. R., Kiel, M., et al. (2023). Exploring bias in the OCO-3 snapshot area mapping mode via geometry, surface, and aerosol effects. *Atmospheric Measurement Techniques*, *16*(1), 109–133. https://doi.org/10.5194/amt-16-109-2023

Bovensmann, H., Burrows, J. P., Buchwitz, M., Frerick, J., Noel, S., Rozanov, V. V., et al. (1999). SCIAMACHY: Mission objectives and measurement modes. *Journal of the Atmospheric Sciences*, *56*(2), 127–150. https://doi.org/10.1175/1520-0469(1999)056<0127:SMOAMM>2.0.CO;2

Butz, A., Guerlet, S., Hasekamp, O., Schepers, D., Galli, A., Aben, I., et al. (2011). Toward accurate CO_2 and CH_4 observations from GOSAT. *Geophysical Research Letters*, *38*(14). https://doi.org/10.1029/2011GL047888

Che, K., Lauvaux, T., Taquet, N., Stremme, W., Xu, Y., Alberti, C., et al. (2024). Urban XCO_2 radients from a dense network of solar absorption spectrometers and OCO-3 over Mexico City. *Journal of Geophysical Research: Atmospheres*, *129*(9), e2023JD040063. https://doi.org/10.1029/2023JD040063

Chen, J., Makowski, M., Luther, A., & Dietrich, F. (2026). MUCCnet XCO_2 network observations during OCO2 and OCO3 overpasses, PROFFAST 1.0 and 2.2, Summer 2020 (1.0.0) [Dataset]. *CaltechDATA*. https://doi.org/10.22002/vacrg-gh9

Connor, B. J., Boesch, H., Toon, G., Sen, B., Miller, C., & Crisp, D. (2008). Orbiting Carbon Observatory: Inverse method and prospective error analysis. *Journal of Geophysical Research*, *113*(D5). https://doi.org/10.1029/2006JD008336

Crisp, D., Atlas, R. M., Breon, F. M., Brown, L. R., Burrows, J. P., Ciais, P., et al. (2004). The orbiting carbon observatory (OCO) mission. *Advances in Space Research*, *34*(4), 700–709. https://doi.org/10.1016/j.asr.2003.08.062

Crisp, D., Miller, C. E., & DeCola, P. L. (2006). The NASA orbiting carbon observatory: Measuring the column-integrated atmospheric CO_2 abundance from Space. In *Sensors, systems, and next-generation satellites X* (Vol. 6361, pp. 117–126). SPIE.

Crisp, D., Miller, C. E., & DeCola, P. L. (2008). NASA orbiting carbon observatory: Measuring the column averaged carbon dioxide mole fraction from space. *Journal of Applied Remote Sensing*, *2*(1), 023508. https://doi.org/10.1117/1.2898457

Crisp, D., Pollock, H. R., Rosenberg, R., Chapsky, L., Lee, R. A., Oyafuso, F. A., et al. (2017). The on-orbit performance of the Orbiting Carbon Observatory-2 (OCO-2) instrument and its radiometrically calibrated products. *Atmospheric Measurement Techniques*, *10*(1), 59–81. https://doi.org/10.5194/amt-10-59-2017

Das, S., Kiel, M., Laughner, J., Osterman, G., O'Dell, C. W., Taylor, T. E., et al. (2025). Comparisons of the v11.1 Orbiting Carbon Observatory-2 (OCO-2) XCO_2 measurements with GGG2020 TCCON. *Earth and Space Science*, *12*(7), e2024EA003935. https://doi.org/10.1029/2024EA003935

Eldering, A., Taylor, T. E., O'Dell, C. W., & Pavlick, R. (2019). The OCO-3 mission: Measurement objectives and expected performance based on 1 year of simulated data. *Atmospheric Measurement Techniques*, *12*(4), 2341–2370. https://doi.org/10.5194/amt-12-2341-2019

Feld, L., Herkommer, B., Vestner, J., Dubravica, D., Alberti, C., & Hase, F. (2024). Proffastpylot: Running proffast with python. *Journal of Open Source Software*, *9*(96), 6481. https://doi.org/10.21105/joss.06481

Fisher, J. B., Lee, B., Purdy, A. J., Halverson, G. H., Dohlen, M. B., Cawse-Nicholson, K., et al. (2020). ECOSTRESS: NASA's next generation mission to measure evapotranspiration from the international space station. *Water Resources Research*, *56*(4), e2019WR026058. https://doi.org/10.1029/2019wr026058

Frey, M., Sha, M. K., Hase, F., Kiel, M., Blumenstock, T., Harig, R., et al. (2019). Building the COllaborative Carbon Column Observing Network (COCCON): Long-term stability and ensemble performance of the EM27/SUN Fourier transform spectrometer. *Atmospheric Measurement Techniques*, *12*(3), 1513–1530. https://doi.org/10.5194/amt-12-1513-2019

Frey, M. M., Hase, F., Blumenstock, T., Dubravica, D., Groß, J., Göttsche, F., et al. (2021). Long-term column-averaged greenhouse gas observations using a COCCON spectrometer at the high-surface-albedo site in Gobabeb, Namibia. *Atmospheric Measurement Techniques*, *14*(9), 5887–5911. https://doi.org/10.5194/amt-14-5887-2021

Gadhavi, H. S., Arora, A., Jain, C., Sha, M. K., Hase, F., Frey, M. M., et al. (2025). Validation and assessment of satellite-based columnar CO_2 and CH_4 mixing ratios from GOSAT and OCO-2 satellites over India. *Atmospheric Measurement Techniques*, *18*(17), 4497–4514. https://doi.org/10.5194/amt-18-4497-2025

support of the measurements in Uganda. Drs. Neil Humpage and Robert Parker acknowledge funding provided by the Natural Environment Research Council (The Global Methane Budget - NE/N015681/1), the UK National Centre for Earth Observation (Grant: NE/W004895/1), a UKRI Future Leaders Fellowship (Grant: MR/X033139/1), and the Greenhouse Gas Emissions Measurement and Modeling Advancement (GEMMA) Programme (NE/Y00177X/1). The Paris site has received funding from Sorbonne Université, the French research center CNRS, and the French space agency CNES. The FTIR measurements at Xianghe and Beijing are supported by the National Key Research and Development Program of China (2023YFB3907505). K.G. was supported by the Ministry of Science and Higher Education of the Russian Federation (project no. FEUZ-2024-0011). The SPbU team is supported by a research project 132392751 (GZ_MDF_2026). Hayoung Park and Sujong Jeong were supported by Korea Environment Industry & Technology Institute (KEITI) through "Climate Change R&D Project for New Climate Regime," funded by Korea Ministry of Environment (MOE) (2022003560006). The Technical University of Munich (TUM) authors would like to acknowledge the funding support by the European Union's Horizon 2020 programme in the framework of the ICOS Cities project (Grant 101037319), the European Research Council (ERC) Consolidator Grant CoSense4Climate (Grant 101089203), and from the German Federal Ministry of Research, Technology and Space (BMFTR) within its project ITMS via Grant 01LK2303B.

Gisi, M., Hase, F., Dohe, S., Blumenstock, T., Simon, A., & Keens, A. (2012). X_{CO_2}-measurements with a tabletop FTS using solar absorption spectroscopy. *Atmospheric Measurement Techniques*, *5*(11), 2969–2980. https://doi.org/10.5194/amt-5-2969-2012

Guan, X., Sun, Z., Chu, D., Xie, G., Wang, Y., & Shen, H. (2024). Long-term (2000–2020) global 0.05° continuous atmospheric carbon dioxide mapping combining OCO-2 observations and model simulations. *Science of the Total Environment*, *957*, 177051. https://doi.org/10.1016/j.scitotenv.2024.177051

Guan, Y., McKinley, G. A., Fay, A. R., Doney, S. C., & Keppel-Aleks, G. (2024). Ocean-driven interannual variability in atmospheric CO_2 quantified using OCO-2 observations and atmospheric transport simulations. *Frontiers in Marine Science*, *11*, 1272415. https://doi.org/10.3389/fmars.2024.1272415

Hall, B. D., Crotwell, A. M., Kitzis, D. R., Mefford, T., Miller, B. R., Schibig, M. F., & Tans, P. P. (2021). Revision of the world meteorological organization global atmosphere watch (WMO/GAW) CO_2 calibration scale. *Atmospheric Measurement Techniques*, *14*(4), 3015–3032. https://doi.org/10.5194/amt-14-3015-2021

Hase, F., Frey, M., Kiel, M., Blumenstock, T., Harig, R., Keens, A., & Orphal, J. (2016). Addition of a channel for XCO observations to a portable FTIR spectrometer for greenhouse gas measurements. *Atmospheric Measurement Techniques*, *9*(5), 2303–2313. https://doi.org/10.5194/amt-9-2303-2016

Herkommer, B., Alberti, C., Castracane, P., Chen, J., Dehn, A., Dietrich, F., et al. (2024). Using a portable FTIR spectrometer to evaluate the consistency of Total Carbon Column Observing Network (TCCON) measurements on a global scale: The Collaborative Carbon Column Observing Network (COCCON) travel standard. *Atmospheric Measurement Techniques*, *17*(11), 3467–3494. https://doi.org/10.5194/amt-17-3467-2024

Jacobs, N., O'Dell, C. W., Taylor, T. E., Logan, T. L., Byrne, B., Kiel, M., & Chatterjee, A. (2024). The importance of digital elevation model accuracy in XCO_2 retrievals: Improving the orbiting carbon observatory 2 atmospheric carbon observations from space version 11 retrieval product. *Atmospheric Measurement Techniques*, *17*(5), 1375–1401. https://doi.org/10.5194/amt-17-1375-2024

Jacobs, N., Simpson, W. R., Wunch, D., O'Dell, C. W., Osterman, G. B., Hase, F., et al. (2020). Quality controls, bias, and seasonality of CO_2 columns in the boreal forest with Orbiting Carbon Observatory-2, Total carbon column observing network, and EM27/SUN measurements. *Atmospheric Measurement Techniques*, *13*(9), 5033–5063. https://doi.org/10.5194/amt-13-5033-2020

Keller, G. R., Rosenberg, R. A., Merrelli, A., O'Dell, C. W., Spiers, G. D., Payne, V. H., & Chatterjee, A. (2025). New inflight calibration of OCO-3's A-band for version 11 products. *IEEE Transactions on Geoscience and Remote Sensing*, *63*, 1–12. https://doi.org/10.1109/tgrs.2025.3532216

Keppel-Aleks, G., Wennberg, P. O., & Schneider, T. (2011). Sources of variations in total column carbon dioxide. *Atmospheric Chemistry and Physics*, *11*(8), 3581–3593. https://doi.org/10.5194/acp-11-3581-2011

Kiel, M., Eldering, A., Roten, D. D., Lin, J. C., Feng, S., Lei, R., et al. (2021). Urban-focused satellite CO_2 observations from the Orbiting Carbon Observatory-3: A first look at the Los Angeles megacity. *Remote Sensing of Environment*, *258*, 112314. https://doi.org/10.1016/j.rse.2021.112314

Kiel, M., O'Dell, C. W., Fisher, B., Eldering, A., Nassar, R., MacDonald, C. G., & Wennberg, P. O. (2019). How bias correction goes wrong: Measurement of XCO_2 affected by erroneous surface pressure estimates. *Atmospheric Measurement Techniques*, *12*(4), 2241–2259. https://doi.org/10.5194/amt-12-2241-2019

Kohtake, N., Katoh, A., Ishihama, N., Miyamoto, Y., Kawasaki, T., & Katahira, M. (2008). Software independent verification and validation for spacecraft at JAXA. In *2008 IEEE aerospace conference* (pp. 1–8). IEEE. https://doi.org/10.1109/AERO.2008.4526598

Kunchala, R. K., Patra, P. K., Kumar, K. N., Chandra, N., Attada, R., & Karumuri, R. K. (2022). Spatio-temporal variability of XCO_2 over Indian region inferred from Orbiting Carbon Observatory (OCO-2) satellite and chemistry transport model. *Atmospheric Research*, *269*, 106044. https://doi.org/10.1016/j.atmosres.2022.106044

Kuze, A., Suto, H., Nakajima, M., & Hamazaki, T. (2009). Thermal and near infrared sensor for carbon observation Fourier-transform spectrometer on the greenhouse gases observing satellite for greenhouse gases monitoring. *Applied Optics*, *48*(35), 6716–6733. https://doi.org/10.1364/AO.48.006716

Kuze, A., Suto, H., Shiomi, K., Kawakami, S., Tanaka, M., Ueda, Y., et al. (2016). Update on GOSAT TANSO-FTS performance, operations, and data products after more than 6 years in space. *Atmospheric Measurement Techniques*, *9*(6), 2445–2461. https://doi.org/10.5194/amt-9-2445-2016

Laughner, J. L., Roche, S., Kiel, M., Toon, G. C., Wunch, D., Baier, B. C., et al. (2023). A new algorithm to generate a priori trace gas profiles for the GGG2020 retrieval algorithm. *Atmospheric Measurement Techniques*, *16*(5), 1121–1146. https://doi.org/10.5194/amt-16-1121-2023

Laughner, J. L., Toon, G. C., Mendonca, J., Petri, C., Roche, S., Wunch, D., et al. (2024). The total carbon column observing network's GGG2020 data version. *Earth System Science Data*, *16*(5), 2197–2260. https://doi.org/10.5194/essd-16-2197-2024

Lei, R., Poe, J., Huntzinger, D., Liu, J., Stich, S., Baker, D. F., et al. (2024). The Orbiting Carbon Observatory-2 (OCO-2) and in situ CO_2 data suggest a larger seasonal amplitude of the terrestrial carbon cycle compared to many dynamic global vegetation models. *Remote Sensing of Environment*, *312*, 114326. https://doi.org/10.1016/j.rse.2024.114326

Lei, T. T., Liu, J., Xia, Q. K., Zhou, J. J., & Luan, Z. K. (2024). Prediction of CO_2 content in mid-ocean ridge basalts via a machine learning approach. *Geology*, *52*(12), 901–905. https://doi.org/10.1130/g52466.1

Liu, Y., Wang, J., Yao, L., Chen, X., Cai, Z., Yang, D., et al. (2018). The TanSat mission: Preliminary global observations. *Science Bulletin*, *63*(18), 1200–1207. https://doi.org/10.1016/j.scib.2018.08.004

Messerschmidt, J., Geibel, M. C., Blumenstock, T., Chen, H., Deutscher, N. M., Engel, A., et al. (2011). Calibration of TCCON column-averaged CO_2: The first aircraft campaign over European TCCON sites. *Atmospheric Chemistry and Physics*, *11*(21), 10765–10777. https://doi.org/10.5194/acp-11-10765-2011

Miller, S. M., Michalak, A. M., Yadav, V., & Tadić, J. M. (2018). Characterizing biospheric carbon balance using CO_2 observations from the OCO-2 satellite. *Atmospheric Chemistry and Physics*, *18*(9), 6785–6799. https://doi.org/10.5194/acp-18-6785-2018

Nassar, R., Mastrogiacomo, J. P., Bateman-Hemphill, W., McCracken, C., MacDonald, C. G., Hill, T., et al. (2021). Advances in quantifying power plant CO_2 emissions with OCO-2. *Remote Sensing of Environment*, *264*, 112579. https://doi.org/10.1016/j.rse.2021.112579

Nguyen, H., & Hobbs, J. (2020). Intercomparison of remote sensing retrievals: An examination of prior-induced biases in averaging kernel corrections. *Remote Sensing*, *12*(19), 3239. https://doi.org/10.3390/rs12193239

OCO-2 Science Team. (2014). The OCO-2 v11.2 XCO_2 (Dry-air mole fraction of carbon dioxide) product [Dataset]. *OCO-2 Science Team*. Retrieved from https://daac.gsfc.nasa.gov/

OCO-3 Science Team. (2019). The OCO-2 v11 XCO_2 (Dry-air mole fraction of carbon dioxide) product [Dataset]. *OCO-2 Science Team*. Retrieved from https://daac.gsfc.nasa.gov/

O'Dell, C. W., Connor, B., Bösch, H., O'Brien, D., Frankenberg, C., Castano, R., et al. (2012). The ACOS CO_2 retrieval algorithm–part 1: Description and validation against synthetic observations. *Atmospheric Measurement Techniques*, *5*(1), 99–121. https://doi.org/10.5194/amt-5-99-2012

O'Dell, C. W., Eldering, A., Wennberg, P. O., Crisp, D., Gunson, M. R., Fisher, B., et al. (2018). Improved retrievals of carbon dioxide from Orbiting Carbon Observatory-2 with the version 8 ACOS algorithm. *Atmospheric Measurement Techniques*, *11*(12), 6539–6576. https://doi.org/10.5194/amt-11-6539-2018

Oyafuso, F., Payne, V. H., Drouin, B. J., Devi, V. M., Benner, D. C., Sung, K., et al. (2017). High accuracy absorption coefficients for the Orbiting Carbon Observatory-2 (OCO-2) mission: Validation of updated carbon dioxide cross-sections using atmospheric spectra. *Journal of Quantitative Spectroscopy and Radiative Transfer*, *203*, 213–223. https://doi.org/10.1016/j.jqsrt.2017.06.012

Park, H., Jeong, S., Sha, M. K., Lee, J., & Frey, M. M. (2024). Comparisons of greenhouse gas observation satellite performances over Seoul using a portable ground-based spectrometer. *Geophysical Research Letters*, *51*(14), e2024GL109334. https://doi.org/10.1029/2024GL109334

Parker, R. J., Webb, A., Boesch, H., Somkuti, P., Barrio Guillo, R., Di Noia, A., et al. (2020). A decade of GOSAT Proxy satellite CH 4 observations. *Earth System Science Data*, *12*(4), 3383–3412. https://doi.org/10.5194/essd-12-3383-2020

Patra, P. K., Hajima, T., Saito, R., Chandra, N., Yoshida, Y., Ichii, K., et al. (2021). Evaluation of Earth system model and atmospheric inversion using total column CO2 observations from GOSAT and OCO-2. *Progress in Earth and Planetary Science*, *8*(1), 25. https://doi.org/10.1186/s40645-021-00420-z

Philip, S., Johnson, M. S., Baker, D. F., Basu, S., Tiwari, Y. K., Indira, N. K., et al. (2022). OCO-2 satellite-imposed constraints on terrestrial biospheric CO2 fluxes over South Asia. *Journal of Geophysical Research: Atmospheres*, *127*(3), e2021JD035035. https://doi.org/10.1029/2021JD035035

Pollard, D. F., Hase, F., Sha, M. K., Dubravica, D., Alberti, C., & Smale, D. (2022). Retrievals of XCO_2, XCH_4 and XCO from portable, near-infrared fourier transform spectrometer solar observations in Antarctica. *Earth System Science Data*, *14*(12), 5427–5437. https://doi.org/10.5194/essd-14-5427-2022

Pollard, D. F., Robinson, J., & Shiona, H. (2022a). TCCON data from Lauder (NZ), Release GGG2020.R0 (version R0) [Dataset]. *CaltechDATA*. https://doi.org/10.14291/TCCON.GGG2020.LAUDER03.R0

Rodgers, C. D., & Connor, B. J. (2003). Intercomparison of remote sounding instruments. *Journal of Geophysical Research*, *108*(D3). https://doi.org/10.1029/2002jd002299

Rosenberg, R., Chapsky, L., Crisp, D., Keller, G., Lee, R., Marchetti, Y., & Eldering, A. (2020). OCO-2 calibration refinement across versions and plans for OCO-3. In *IGARSS 2020-2020 IEEE international geoscience and remote sensing symposium* (pp. 6381–6384).

Sha, M. K., Das, S., Frey, M. M., Dubravica, D., Alberti, C., Baier, B. C., et al. (2025). Fiducial reference measurements for greenhouse gases (FRM4GHG): Validation of satellite (Sentinel-5 precursor, OCO-2, and GOSAT) missions using the COllaborative Carbon Column Observing Network (COCCON). *Remote Sensing*, *17*(5), 734. https://doi.org/10.3390/rs17050734

Sha, M. K., De Mazière, M., Notholt, J., Blumenstock, T., Chen, H., Dehn, A., et al. (2020). Intercomparison of low-and high-resolution infrared spectrometers for ground-based solar remote sensing measurements of total column concentrations of CO_2, CH_4, and CO. *Atmospheric Measurement Techniques*, *13*(9), 4791–4839. https://doi.org/10.5194/amt-13-4791-2020

Sha, M. K., De Mazière, M., Notholt, J., Blumenstock, T., Bogaert, P., Cardoen, P., et al. (2024). Fiducial reference measurement for greenhouse gases (frm4ghg). *Remote Sensing*, *16*(18), 3525. https://doi.org/10.3390/rs16183525

Shekhar, A., Chen, J., Paetzold, J. C., Dietrich, F., Zhao, X., Bhattacharjee, S., et al. (2020). Anthropogenic CO_2 emissions assessment of Nile Delta using XCO_2 and SIF data from OCO-2 satellite. *Environmental Research Letters*, *15*(9), 095010. https://doi.org/10.1088/1748-9326/ab9cfe

Taylor, T. E., O'Dell, C. W., Baker, D., Bruegge, C., Chang, A., Chapsky, L., & Zong, J. (2023). Evaluating the consistency between OCO-2 and OCO-3 XCO_2 estimates derived from the NASA ACOS version 10 retrieval algorithm. *Atmospheric Measurement Techniques Discussions*, *2023*, 1–61. https://doi.org/10.5194/amt-2022-329

Thompson, D. R., Benner, D. C., Brown, L. R., Crisp, D., Devi, V. M., Jiang, Y., et al. (2012). Atmospheric validation of high accuracy CO_2 absorption coefficients for the OCO-2 mission. *Journal of Quantitative Spectroscopy and Radiative Transfer*, *113*(17), 2265–2276. https://doi.org/10.1016/j.jqsrt.2012.05.021

Veefkind, J. P., Aben, I., McMullan, K., Förster, H., De Vries, J., Otter, G., et al. (2012). TROPOMI on the ESA Sentinel-5 precursor: A GMES mission for global observations of the atmospheric composition for climate, air quality and ozone layer applications. *Remote Sensing of Environment*, *120*, 70–83. https://doi.org/10.1016/j.rse.2011.09.027

Villalobos, Y., Rayner, P. J., Silver, J. D., Thomas, S., Haverd, V., Knauer, J., et al. (2021). Was Australia a sink or source of CO_2 in 2015? Data assimilation using OCO-2 satellite measurements. *Atmospheric Chemistry and Physics*, *21*(23), 17453–17494. https://doi.org/10.5194/acp-21-17453-2021

Vogel, F. R., Frey, M., Staufer, J., Hase, F., Broquet, G., Xueref-Remy, I., et al. (2019). X_{CO_2} in an emission hotspot region: The COCCON Paris campaign 2015. *Atmospheric Chemistry and Physics*, *19*(5), 3271–3285. https://doi.org/10.5194/acp-19-3271-2019

Wang, S., van der A, R. J., Stammes, P., Wang, W., Zhang, P., Lu, N., et al. (2020). Carbon dioxide retrieval from TanSat observations and validation with TCCON measurements. *Remote Sensing*, *12*(14), 2204. https://doi.org/10.3390/rs12142204

Wei, C., Lyu, Z., Bu, L., & Liu, J. (2022). Occurrence and discrepancy of surface and column mole fractions of CO_2 and CH_4 at a desert site in Dunhuang, Western China. *Atmosphere*, *13*(4), 571. https://doi.org/10.3390/atmos13040571

Wunch, D., Toon, G. C., Blavier, J. F. L., Washenfelder, R. A., Notholt, J., Connor, B. J., et al. (2011). The total carbon column observing network. *Philosophical Transactions of the Royal Society A: Mathematical, Physical & Engineering Sciences*, *369*(1943), 2087–2112. https://doi.org/10.1098/rsta.2010.0240

Wunch, D., Toon, G. C., Wennberg, P. O., Wofsy, S. C., Stephens, B. B., Fischer, M. L., et al. (2010). Calibration of the Total Carbon Column Observing Network using aircraft profile data. *Atmospheric Measurement Techniques*, *3*(5), 1351–1362. https://doi.org/10.5194/amt-3-1351-2010

Wunch, D., Wennberg, P. O., Osterman, G., Fisher, B., Naylor, B., Roehl, C. M., & Eldering, A. (2017). Comparisons of the orbiting carbon observatory-2 (OCO-2) XCO_2 measurements with TCCON. *Atmospheric Measurement Techniques*, *10*(6), 2209–2238. https://doi.org/10.5194/amt-10-2209-2017

Wunch, D. W. P. O., Wennberg, P. O., Toon, G. C., Connor, B. J., Fisher, B., Osterman, G. B., et al. (2011). A method for evaluating bias in global measurements of CO_2 total columns from space. *Atmospheric Chemistry and Physics*, *11*(23), 12317–12337. https://doi.org/10.5194/acp-11-12317-2011

Yang, D., Liu, Y., Cai, Z., Chen, X., Yao, L., & Lu, D. (2018). First global carbon dioxide maps produced from TanSat measurements

Yang, L., Wang, Y., Dong, G., Gu, H., Huang, J., Zhu, J., et al. (2007). The impact of free-air CO_2 enrichment (FACE) and nitrogen supply on grain quality of rice. *Field Crops Research*, *102*(2), 128–140. https://doi.org/10.1016/j.fcr.2007.03.006

Yokota, T., Yoshida, Y., Eguchi, N., Ota, Y., Tanaka, T., Watanabe, H., & Maksyutov, S. (2009). Global concentrations of CO_2 and CH_4 retrieved from GOSAT: First preliminary results. *Inside Solaris*, *5*, 160–163. https://doi.org/10.2151/sola.2009-041

Zhou, M., & Cai, Z. (2026). OCO-2 and -3 coincident days v1 COCCON data from Beijing and Xianghe (1.0.0) [Dataset]. *CaltechDATA*. https://doi.org/10.22002/cfhma-1xr56